nature chemistry

ARTICLES

PUBLISHED ONLINE: 10 APRIL 2017 | DOI: 10.1038/NCHEM.2759

Chelation and stabilization of berkelium in oxidation state +IV

Gauthier J.-P. Deblonde[1], Manuel Sturzbecher-Hoehne[1], Peter B. Rupert[2], Dahlia D. An[1], Marie-Claire Illy[1], Corie Y. Ralston[3], Jiri Brabec[4], Wibe A. de Jong[5]*, Roland K. Strong[2]* and Rebecca J. Abergel[1]*

Berkelium (Bk) has been predicted to be the only transplutonium element able to exhibit both +III and +IV oxidation states in solution, but evidence of a stable oxidized Bk chelate has so far remained elusive. Here we describe the stabilization of the heaviest 4+ ion of the periodic table, under mild aqueous conditions, using a siderophore derivative. The resulting Bk(IV) complex exhibits luminescence via sensitization through an intramolecular antenna effect. This neutral Bk(IV) coordination compound is not sequestered by the protein siderocalin—a mammalian metal transporter—in contrast to the negatively charged species obtained with neighbouring trivalent actinides americium, curium and californium (Cf). The corresponding Cf(III)–ligand–protein ternary adduct was characterized by X-ray diffraction analysis. Combined with theoretical predictions, these data add significant insight to the field of transplutonium chemistry, and may lead to innovative Bk separation and purification processes.

Berkelium (Bk) chemistry is largely unexplored compared with other transplutonium elements encountered in measurable amounts in nuclear chemistry, namely americium (Am), curium (Cm), and californium (Cf). Element 97, Bk is a peculiar case in the actinide (An) series because it is 'light' enough to be formed by multiple neutron-capture processes during nuclear detonations or in today's nuclear fission reactors, to such extent that it raises concerns for nuclear waste management[1,2]. However, its only isotope available in bulk quantities, ^{249}Bk, has a relatively short half-life of 330 days, which hinders its use in chemical studies. In contrast, ^{243}Am ($t_{1/2}$ = 7,370 yr) and ^{248}Cm ($t_{1/2}$ = 340,000 yr) are long-lived isotopes that can be produced and purified on the multi-gram scale. Likewise, Cf (Z = 98), although heavier than Bk, is easier to synthesize and investigate thanks to the relatively stable isotopes ^{249}Cf ($t_{1/2}$ = 351 yr) and ^{252}Cf ($t_{1/2}$ = 2.65 yr). A consequence of its extreme rarity as a laboratory material and its highly radioactive nature, very few Bk coordination compounds have been characterized to date[3,4] and little is known about the behaviour of Bk in environmentally and biologically relevant species[5,6]. Due to the special stability afforded by the half-filled $5f^7$ electronic configuration, Bk is the element among the actinides heavier than plutonium (Pu) that can most readily be oxidized from oxidation state +III to +IV in aqueous systems; its neighbouring elements, Am, Cm, Cf and einsteinium (Es) having only limited or inexistent stability as M(IV) ions[7]. Even though rutherfordium (Rf, Z = 104) is expected to exhibit coordination chemistry properties similar to those of zirconium (Zr) and hafnium (Hf) and would therefore also readily form a stable M(IV) ion in solution[8], its isotopes are short-lived (with half-lives from μs to ~1.3 hours) and Bk is, until now, the heaviest element of the periodic table available for bulk chemistry that can be studied as a tetravalent ion. It preferentially exists in aqueous solutions as Bk(III) but oxidation to Bk(IV) under very drastic conditions was reported shortly after the discovery of the element[9,10]. The standard oxidation potential for the couple Bk^{4+}/Bk^{3+} is +1.60 V (in 1 M $HClO_4$ versus NHE)[11], which makes the formation of Bk(IV) species arduous, yet feasible, with a large excess of very strong oxidizers such as bromate, bismuth trioxide and lead dioxide, or by prolonged electrolytic oxidation. The redox properties of Bk are relatively close to those of cerium (Ce, $E°_{Ce^{4+}/Ce^{3+}}$ = +1.7 V) and differ significantly from what is observed with the corresponding lanthanide (Ln) ion, terbium (Tb, $E°_{Tb^{4+}/Tb^{3+}}$ = +3.3 V) (ref. 12). This ambivalence, if adequately unlocked, would confer to Bk a chemical behaviour readily different from that of adjacent ions, Cm and Cf, whose only stable oxidation state in solution is +III.

Classical attempts to extend the chemistry of Bk have yielded a decrease of the Bk^{4+}/Bk^{3+} potential to +1.56 V in 1 M HNO_3 and +1.37 V in 1 M H_2SO_4 (refs 3,13). An almost identical trend is known for the couple Ce^{4+}/Ce^{3+}, whose redox potential is +1.70 V, +1.61 V, +1.44 V and +1.28 V in 1 M $HClO_4$, HNO_3, H_2SO_4 and HCl, respectively[14]. The difference in stability between the Bk(IV) and Bk(III) species formed with these common anions is, however, not strong enough to make Bk(IV) readily accessible. In fact, once tremendous efforts are made to oxidize Bk(III) in these mineral acids, Bk(IV) complexes are naturally reduced within a few hours or even minutes[15–17]. More exotic approaches to stabilize Bk(IV) have used saturated pyrophosphate solutions[17], acidic mixtures of bromate and heteropolytungstate $K_{10}P_2W_{17}O_{61}$ (ref. 18), or triphenylarsine oxide in pure acetonitrile[19], all transient and difficult systems to implement in separation processes or for the sequestration of Bk *in vivo*. A more realistic strategy was proposed in the early 1970s using highly concentrated carbonate solutions[13,16], with a conditional oxidation potential Bk^{4+}/Bk^{3+} of +0.26 V in 2 M K_2CO_3 (pH 10). Aside from requiring a tremendous excess of carbonate ions, this medium's drawbacks include a narrow

[1]Chemical Sciences Division, Lawrence Berkeley National Laboratory, Berkeley, California 94720, USA. [2]Division of Basic Science, Fred Hutchinson Cancer Research Center, Seattle, Washington 98109, USA. [3]Berkeley Center for Structural Biology, Lawrence Berkeley National Laboratory, Berkeley, California 94720, USA. [4]J. Heyrovsky Institute of Physical Chemistry, Academy of Sciences of the Czech Republic, 18223 Prague 8, Czech Republic. [5]Computational Research Division, Lawrence Berkeley National Laboratory, Berkeley, California 94720, USA. *e-mail: wadejong@lbl.gov; rstrong@fhcrc.org; rjabergel@lbl.gov

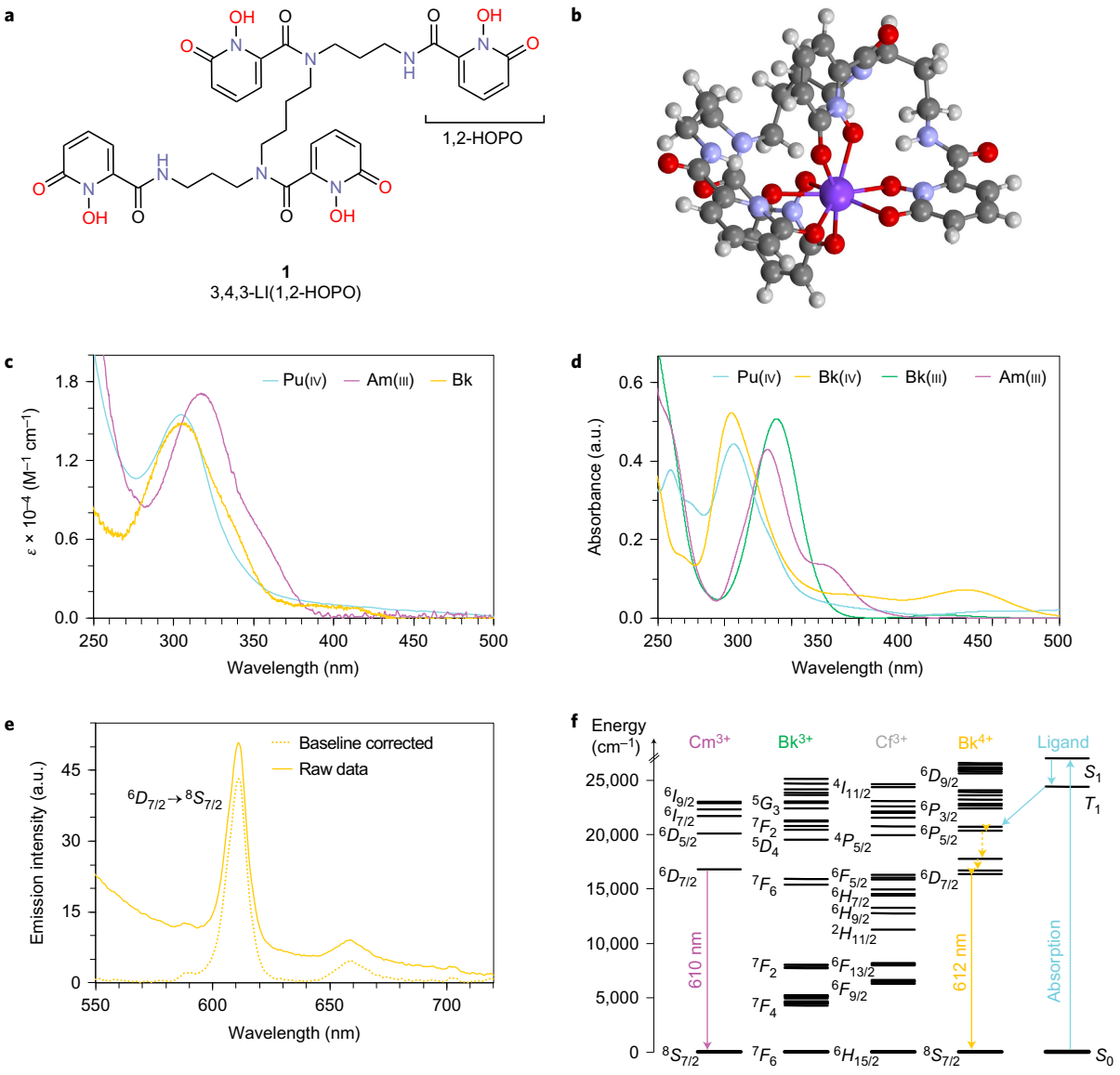

Figure 1 | Stabilization and sensitization of Bk(IV) were achieved through chelation with a siderophore derivative. a, Molecular structure of 3,4,3-LI(1,2-HOPO) (**1**, hydrogen atoms highlighted in red are labile), the ligand used to chelate Bk(IV) and form a stable complex [Bk(IV)**1**]. **b**, Computed DFT structure of [Bk(IV)**1**]. **c**,**d**, Experimental absorbance spectra of **1** complexed with Pu(IV) (blue), Am(III) (magenta) and Bk (yellow) in aqueous solution (**c**) and computed absorbance spectra for the Pu(IV) (Supplementary Table 8), Bk(IV) yellow, Bk(III) (green) and Am(III) (Supplementary Table 9) complexes (**d**) evidence a shift of maximum absorption between M(III) and M(IV) species. Excitation of [^{249}Bk(IV)**1**] at 320 nm (0.1 M CHES buffer, pH 8.4, 25 °C) results in steady-state emission. **e**, Consistent with sensitization through energy transfer, as expected from the ligand and metal energy levels of the ligand and metal ions displayed in the Jablonski diagrams. **f**, Respective Bk^{4+} and An^{3+} energy levels correspond to those reported for Bk(IV)-doped $CeF_{4(s)}$ (ref. 31) and for $AnCl_3$ or An(III)-doped $LaCl_{3(s)}$ (ref. 32).

pH-range under which Bk(IV) species are stable, the presence of multiple species with unknown stoichiometry or stability[20], the limited solubility of carbonate salts, and its incompatibility with *in vivo* conditions or most nuclear waste treatment operations in acidic media.

Instead of using large excesses of inorganic complexing ions, we selected a water-soluble small organic molecule that is highly selective toward An(IV) ions in order to lift the thermodynamic barrier imposed by the high redox potential of the couple Bk^{4+}/Bk^{3+}. The synthetic siderophore analogue 3,4,3-LI(1,2-HOPO) (**1**, Fig. 1), composed of 1-hydroxy-pyridine-2-one (1,2-HOPO) units linked to a central linear spermine scaffold, is gaining attention as a therapeutic decorporation agent for its bio-compatibility, its low toxicity[21–23], and its strong efficiency at sequestering actinide and lanthanide ions, including UO_2^{2+}, Ln^{3+}, An^{3+}, Th^{4+} and Pu^{4+} (refs 24–27). The hard donor octadentate ligand **1** binds *d*- and *f*-block metal ions through its four 1-hydroxy-pyridine-2-one (1,2-HOPO) functionalities with extremely high affinities (Supplementary Table 1). Besides its ability to chelate both M(III) and M(IV) ions, a critical advantage of **1** is the stability difference between its M(III) and M(IV) complexes, as epitomized by the Ce(III) complex that exhibits a formation constant of $10^{+17.4}$, 24 orders of magnitude lower than that of its Ce(IV) counterpart ($10^{+41.5}$) (ref. 28). This strong stabilization of Ce(IV), with a free energy of formation of −240 kJ mol^{-1} compared with −99.3 kJ mol^{-1} for the Ce(III) complex, compensates the energetic barrier imposed by the redox potential of Ce^{4+}/Ce^{3+} (124 kJ mol^{-1}) for the free ion. Thus the redox potential of the [Ce(IV)**1**]/[Ce(III)**1**]$^-$ system decreases to −0.02 V (ref. 28), from the free ion's +1.28 V. So far, no other man-made ligand combines such high stability

for both M(III) and M(IV) complexes with extreme selectivity toward M(IV) ions.

Results and Discussion

Bk redox potentials are usually 50–100 mV lower than their Ce counterparts[3], the redox potential for [Bk(IV)**1**]/[Bk(III)**1**]$^-$ is expected to be around −0.1 V (versus NHE), suggesting an easy and direct access to Bk(IV) in solution. This estimated value was confirmed by density functional theory (DFT) calculations on both gas-phase and solvated Bk(III) and Bk(IV) species, for which coordinates and frequencies of the calculated species are listed in Supplementary Tables 2–7; in those solvated species, a Bk^{4+}/Bk^{3+} electrochemical potential with an upper bound of −0.13 V relative to NHE was determined. Considering trends in actinide ionic radii[29] and corresponding Th(IV) and Pu(IV) complex stability constants, a formation constant of $10^{+44.7}$ (at 25 °C) is estimated for [Bk(IV)**1**], a drastic increase over [Bk(III)DTPA]$^{2-}$ (DTPA = diethylenetriaminepentaacetic acid, $\log(\beta_{110}) = 22.8$) and [Bk(III)DPA_3]$^{3-}$ (DPA = dipicolinic acid, $\log(\beta_{130}) = 23.1$), currently the most stable known Bk coordination compounds[4,30]. Rigorous metal- or ligand-competition assays commonly used to determine thermodynamic constants for other 4+ metal complexes cannot be applied to Bk(IV) as they would necessitate a competing ligand that could stabilize Bk(IV) once released by **1** with a known affinity for Bk(IV). Such a system is currently unavailable, because **1** is the first organic ligand reported to stabilize Bk(IV) and no thermodynamic stability constant for a Bk(IV) aqueous species has ever been established.

Photophysical properties of chelated Bk(IV). Stabilization of Bk(IV) by **1** was first indicated by UV–visible spectrophotometry. A striking difference is observed between the An(III) and An(IV) complexes, with respective absorbance bands centred at 318 and 305 nm, as shown for Am(III) and Pu(IV) (Fig. 1c), and the Bk species displaying a maximum absorbance at 305 nm for this sharp band characteristic of the 1,2-HOPO π-π^* transitions. In addition, the Bk complex exhibits a ligand-to-metal charge transfer band centred at 400 nm, a feature also observed with Pu(IV) and Ce(IV) complexes[26,28]. Absorbance spectrum assignment to Bk(IV) was further corroborated by theoretical calculations (Fig. 1d). Luminescence properties have long proven instrumental for actinide complex characterization but most studies focused on Cm species, owing to the $5f^7$ electronic configuration and intrinsically intense $^6D_{7/2} \rightarrow {}^8S_{7/2}$ emission of Cm(III), which facilitates direct excitation of *f*–*f* transitions. Luminescence studies of Bk species are scarce and limited to the solid-state[31,32], with the exception of a report on Bk(III) luminescence in 0.5 M DCl (ref. 33). Characterization of [Bk(IV)**1**] provided the first Bk(IV) luminescence spectral features in aqueous solution via intramolecular sensitization through the so-called antenna effect: ligand excitation at 320 nm resulted in sharp emission peaks at 590, 612, 659 and 702 nm, with the most intense centred at 612 nm (Fig. 1e). The corresponding excitation spectrum monitoring emission at 612 nm displayed a main transition centred at 305 nm (Supplementary Fig. 1) and characteristic of energy transfer from the ligand 1,2-HOPO units[27]. The observed structured four-peak emission is due to ligand field splitting of the emitting state, $J = 7/2$, as the spherical symmetry of the half-filled $5f^7$ configuration should only result in a small splitting (945 cm^{-1} between the lowest and highest Stark levels for the free ion versus 2,700 cm^{-1} for the chelated ion). Interestingly, the bathochromic shift of the emission maxima typically observed during complexation of lanthanide and actinide ions appears very pronounced here: from the highest to the lowest Stark levels of the excited state $^6D_{7/2}$, shifts of ~10 to 90 nm (equivalent to energy shifts of up to 2,100 cm^{-1} or roughly 12%) were observed in the complexation of Bk by **1**. While large shifts (on the order of ~50 nm, or ~1,100 cm^{-1}) have been noted in 5*f* systems before[34], the relative decrease in inter-electronic repulsion in this Bk species is remarkable, especially when compared with the corresponding Am(III) (ref. 27) and Cm(III) (ref. 25) species that displayed respective relative shifts of the order of 1 and 2.5%.

These features bestow additional evidence of the stabilization of Bk(IV) by **1** since, based-on the reported energy levels of Bk(III), the ligand cannot sensitize Bk(III) (Fig. 1f). Correspondingly, excitation of the ligand in [Cf(III)**1**]$^-$ did not result in any luminescence features, as expected from the energy levels of Cf(III). The main emission of [Bk(IV)**1**] (612 nm, $\Phi = 1.2 \times 10^{-5}$) is consistent with the 611 fluorescence band reported for solid Bk-doped CeF_4 after direct excitation[31] and is close to, but completely distinct from, that reported for the isoelectronic Cm(III) complex (610 nm, $\Phi = 0.45$) (ref. 25). Despite the similar half-filled $5f^7$ configurations of both metal ions, the stronger spin-orbit coupling associated with Bk(IV) ($\zeta = 3{,}244$ for the free ion[35]) gives rise to metal-centred electronic energy levels closer to each other than in the case of Cm(III) ($\zeta = 2{,}889$)[36]. Hence the much lower ligand-to-metal energy transfer efficiency observed for the Bk(IV) species is most likely due to the induced presence of a large number of non-emissive energy levels between the ligand triplet excited state and the metal $^6D_{7/2}$ emitting state (Fig. 1f). The Bk(IV) complex displayed a bi-exponential luminescence decay (Supplementary Fig. 2) with two distinct lifetimes (188 ± 19 µs and 6.7 ± 0.9 µs), both increasing slowly but linearly with D_2O content in solution (Supplementary Table 10) and shorter than but in the same range as that of the Cm(III) complex (383 ± 38 µs), consistent with a slightly smaller gap between the $^6D_{7/2}$ emitting and $^8S_{7/2}$ accepting levels for Bk.

Oxidation state confirmation by mass spectrometry. The Bk oxidation state when bound to **1** was unambiguously assigned through liquid chromatography (LC) coupled with high-resolution mass spectrometry (MS). Analysis of 1:1 metal:ligand aqueous mixtures prepared under ambient conditions with ^{241}Am(III), ^{248}Cm(III) and ^{249}Cf(III), whose M^{4+}/M^{3+} redox potentials are extremely high (+2.6, +3.1 and + 3.2 V, respectively)[7,37] confirmed the formation of trivalent complexes of **1**. For those three transplutonium elements, MS patterns are almost identical, with four mono-charged adducts detected ([M(III)LH_2]$^+$, [M(III)LHNa]$^+$, [M(III)LNa_2]$^+$ and [M(III)LNaK]$^+$), which clearly contrasts with the data obtained for tetravalent ^{242}Pu and ^{232}Th complexes (Fig. 2; Supplementary Fig. 3). The MS spectrum of the ^{249}Bk system assembled *in situ* from a Bk(III)Cl_3 solution displayed [BkLH]$^+$, [BkLNa]$^+$ and [BkLK]$^+$ species, demonstrating that the resulting complex contains a Bk(IV) ion and not Bk(III). Spontaneous stabilization of Bk(IV) is thought to occur through air oxidation, similarly to the Ce system, which does not necessitate the addition of oxidizers or the electrolytic oxidation required in previously proposed methods. The use of **1** as a chelation and oxidation-promoting agent for Bk(III) also has the notable advantage of promoting the formation of M(IV) species over a wide pH-range: the Zr(IV), Ce(IV) and Pu(IV) complexes are formed in 1 M H_2SO_4 (ref. 26) and are stable up to pH 11 (Supplementary Fig. 4). Finally, the very high formation constants of the [M(IV)**1**] complexes prevent competition with any ligand potentially present in the media, which gives more flexibility and robustness to the system.

Siderocalin-based macromolecular recognition. Stabilization of Bk(IV) by **1** was further confirmed using secondary macromolecular recognition. The human protein siderocalin (Scn), known to intercept ferric complexes of microbial siderophores as an immune response against bacterial invasion and recently highlighted as a potential player in actinide mammalian uptake, specifically recognizes negatively charged Ln(III), Am(III) and Cm(III) complexes of **1** (ref. 38) through tight electrostatic interactions, but not the

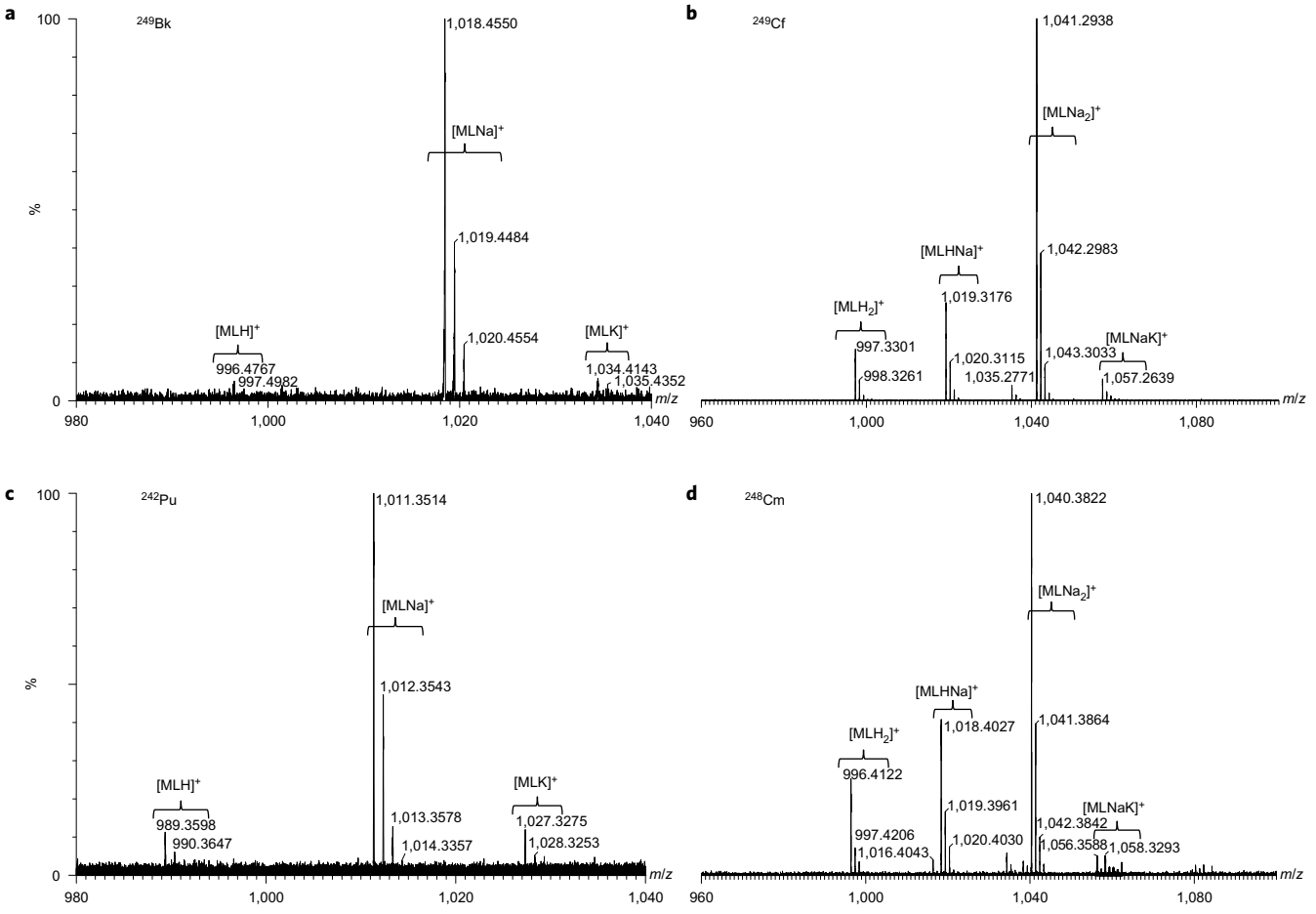

Figure 2 | Mass spectrometry provided definitive evidence of the oxidation state +IV for the Bk species formed with ligand 1. a–d, High-resolution mass spectra of stoichiometric solutions of **1** containing an equivalent of metal are shown for ^{249}Bk (**a**), ^{249}Cf (**b**), ^{242}Pu (**c**) or ^{248}Cm (**d**), with ions detected in positive mode. The four mono-charged adducts detected in the ^{249}Cf(III) and ^{248}Cm(III) systems ($[MLH_2]^+$, $[MLHNa]^+$, $[MLNa_2]^+$ and $[MLNaK]^+$) contrast with those detected for ^{249}Bk and ^{242}Pu(IV) ($[MLH]^+$, $[MLNa]^+$ and $[MLK]^+$).

neutral Th(IV) and Pu(IV) analogues. A fluorescence quenching assay revealed Scn does not recognize Bk–**1**, evidencing the complex neutrality and indirectly confirming the stabilization of Bk(IV) and not Bk(III) by **1**. In contrast, $[Cf(III)\mathbf{1}]^-$-bound Scn with an equilibrium dissociation constant K_d of 50 ± 5 nM, which is in the same range as those reported for Am(III) and Cm(III) (29 and 22 nM, respectively)[38]. The structure of the $[^{249}Cf(III)\mathbf{1}]^-$/Scn ternary complex was determined (Supplementary Table 11) using methods analogous to those derived for corresponding lanthanide (Sm) and actinide (^{243}Am, ^{248}Cm) metal/chelator/Scn adducts[38]; it is the first crystallographic report of a macromolecular Cf assembly. Those prior structures demonstrated that octadentate complexes bind the trilobal Scn ligand binding site, or 'calyx', much as native ferric siderophore complexes do, with 1,2-HOPO units fitting snuggly into sub-pockets within the calyx (Fig. 3a). The overall ^{249}Cf(III) structure is very similar, particularly with regard to the protein (Fig. 3b). However, in detail, the 1,2-HOPO subunits of the chelator showed much more variability among the three views of the $[^{249}Cf(III)\mathbf{1}]^-$ complex ($z = 3$) than among the 18 near-identical views (six per crystallographic asymmetric unit, $z = 6$) of the previous three complex structures (Sm, ^{243}Am, ^{248}Cm; Fig. 3c). The octadentate coordination around the Sm, ^{243}Am, and ^{248}Cm centres that was best described as a 'snub disphenoid' was altered in the case of ^{249}Cf, resulting in incomplete coordination of the ^{249}Cf(III) centre by two of the 1,2-HOPO groups; probably due to different bond lengths between metals and 1,2-HOPO groups constrained to bind within the rigid calyx (Supplementary Table 11). The coordination differences between the Sm and ^{249}Cf structures are noteworthy, as both metal ions are comparably sized[39], and suggest that the Cf 5*f* orbitals may participate in increased orbital mixing.

Protein- and ligand-based separation of Bk. Current processes to separate Bk from Am, Cm, Cf, and fission products after production necessitate numerous steps and use strong oxidizers such as bromate to segregate Bk(IV) from the non-tetravalent ions[3]. Liquid–liquid extraction steps involving mixed mineral acid and organic solvents as well as multiple final separation steps using ion-exchange columns are almost always included in those processes[3,40], even in the case of more recently reported rapid separation techniques[41]. The non-recognition of [Bk(IV)**1**] by Scn suggests innovative procedures to separate Bk from M(III) ions could consist of passing a solution of the irradiated mixture complexed with **1** through a Scn-containing medium, followed by discrimination using either size, mass, affinity, polarity or solubility differences. However, the separation of Bk(IV) from other M(IV) ions potentially present during Bk production, namely Zr, Ce, Th and Pu, also presents a challenge. The Ce–Bk pair is currently known as the most difficult due to the almost-identical redox properties of the two elements[3], which has led to complicated solvent extraction or ion exchange techniques[42–46]. Figure 3d displays the relative retention of various M(IV) complexes of **1** on a classical C_{18} LC column. The retention time of the Bk complex falls between those of Zr(IV) and Ce(IV), trending with the ionic radii of the octa-coordinated metals

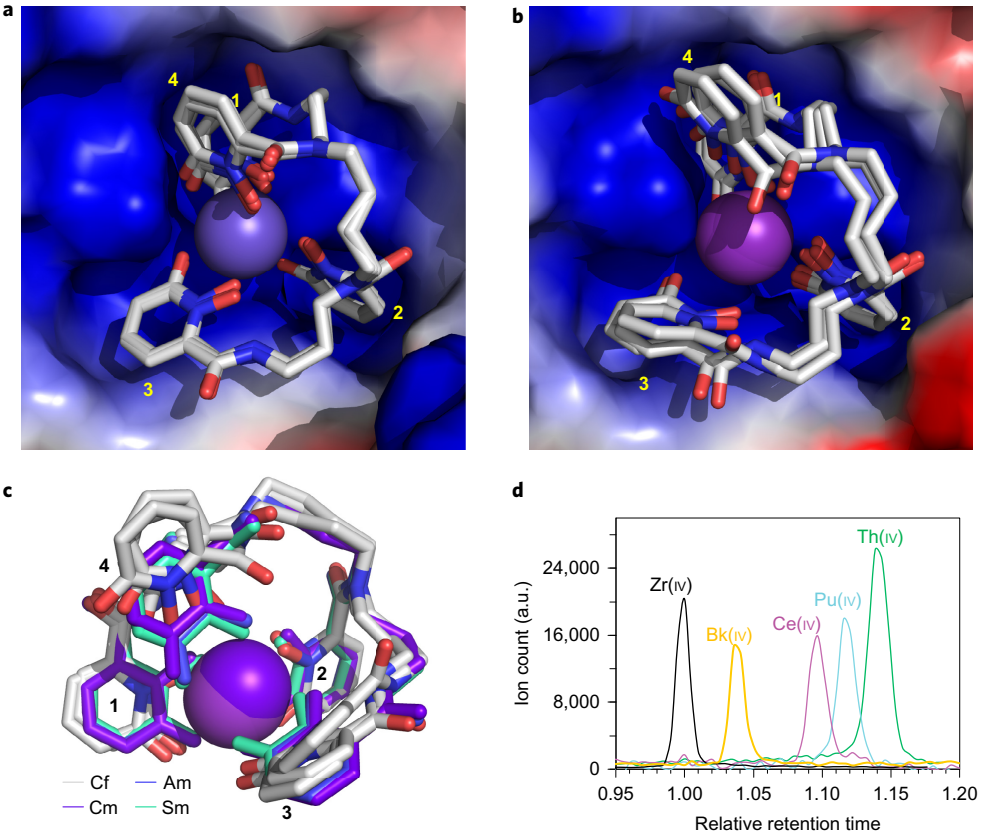

Figure 3 | The selectivity of Scn toward [M(III)1]$^-$ complexes and the different polarity of [M(IV)1] complexes can be used to discriminate Bk from other metal ions. a, Views of previous Scn/[M(III)**1**]$^-$ complex structures show a high degree of structural conservation, with the metal centres (^{243}Am(III), ^{248}Cm(III), Sm(III)) rendered as CPK spheres, the chelator represented by sticks, and the molecular surface of Scn coloured by electrostatic potential (blue: positive; red: negative). Only one of six independent views from each of the three separate structures is shown in this superposition. 1,2-HOPO groups are numbered, with group 1 sitting in the key pocket defining the Scn recognition mechanism[38], partially obscured in this orientation. **b**, Views of the superposition of the three complexes in the asymmetric unit of the Scn/[^{249}Cf(III)**1**]$^-$ structure, rendered as in **a**, show a greater degree of structural variation among the three ^{249}Cf complexes in the crystal than across the three previous complex structures. The no. 4 1,2-HOPO group is clearly displaced outwards from the calyx. **c**, A superposition, based on the structures of Scn, shows the structural differences between one each of the ^{243}Am(III), ^{248}Cm(III), and Sm(III) complexes of **1** (coloured as indicated) and the three [^{249}Cf(III)**1**]$^-$ complexes (coloured by atom type). Incomplete coordination of the ^{249}Cf atom by the no. 3 and 4 1,2-HOPO groups is apparent. **d**, Relative chromatographic retention of [^{249}Bk(IV)**1**], [Ce(IV)**1**], [^{242}Pu(IV)**1**], and [^{232}Th(IV)**1**], relative to [Zr(IV)**1**], on an XDB-C18 column. Detection achieved by mass spectrometry (m/z = 859 (Zr); 909 (Ce); 1,001 (Th); 1,011 (Pu); 1,018 (Bk)).

(0.84, 0.93, and 0.97 pm for Zr(IV), Bk(IV) and Ce(IV), respectively)[29]. Without actual optimization, [Bk(IV)**1**] was easily discriminated from its Ce, Th and Pu analogues. Hence, a two-step separation process is sufficient for isolating Bk from all other lanthanide and actinide ions, with step 1 sequestering 3+ ions based on Scn selectivity toward [M(III)**1**]$^-$ complexes, and step 2 separating Bk from 4+ ions under classical chromatography. Besides stabilizing the heaviest +IV ion of the periodic table available for bulk chemistry, this procedure represents tremendous progress for Bk chemistry as it keeps Bk species in aqueous phase throughout the process, is operated at room temperature and does not introduce additional non-volatile elements or require any biphasic liquid–liquid extraction step, with limiting variables such as solvent loading capacity, pH robustness, extractant solubility, third-phase formation, etc. Recovery of Bk from the final eluted solutions would be achieved either through acidification and ashing or by precipitation of Bk-hydroxide species upon pH increase and subsequent filtration. Both methods (ashing or precipitation), commonly used in hydrometallurgy and would allow recovery of solid Bk. Finally, the protein/ligand-based separation strategy described here could be used to design cleaner and softer methods for metal-ion sorting based on bioengineered systems.

Methods

Caution. ^{249}Cf (351 yr half-life; 4.1 Ci g^{-1}) represents a serious health risk owing to its α emission (6.194 MeV), its γ emission (0.388 MeV), and emission from its decay products such as ^{245}Cm (8,500 yr half-life), an α emitter (5.623 MeV) that undergoes spontaneous fission. ^{249}Bk (330 d half-life) is a β emitter that decays to ^{249}Cf. ^{248}Cm (3.49×10^5 yr half-life; 5.162 MeV) and ^{242}Pu (3.74×10^5 yr half-life ; 4.985 MeV) are α emitters. All these elements where manipulated in laboratories designed for the safe handling of transuranics.

Materials. Chemicals were acquired commercially and used as received. Ligand **1** was prepared and characterized as previously described[47]. Stock solutions (4 mM) of **1** were prepared by dissolution of a weighed portion of ligand in DMSO and aliquots were removed prior to each experiment. Aliquots of acidified stocks of carrier-free ^{249}Cf and ^{248}Cm from the Lawrence Berkeley National Laboratory were used. A stock solution of ^{249}Bk(III) in 0.1 M HCl was prepared from solid $^{249}BkCl_3$ obtained from the Oak Ridge National Laboratory. All measurements were completed within six weeks of the original separation work and within two weeks of dissolution of the dry salt. All aqueous solutions were prepared using deionized water purified by a Millipore Milli-Q reverse osmosis cartridge system and the pH was adjusted as needed with concentrated HCl or KOH. For direct spectroscopic measurements, equimolar amounts of metal and chelator were used to constitute complex solutions (40 μM, pH 8.4) in 0.1 M CHES buffer. Recombinant human Scn was prepared as previously described[48].

Liquid chromatography–mass spectrometry. Liquid chromatography–high resolution mass spectra (LC–HRMS) were acquired on a UPLC Waters Xevo system

interfaced with a QTOF mass spectrometer (Waters Corporation, Milford, Massachusetts, USA) in Micromass Z-spray geometry. The previously described experimental setting[26] used for LC–HRMS assays is detailed in Supplementary Information and was applied to samples containing an equal concentration of actinide and **1** in 0.1 M HEPES buffer (4-(2-hydroxyethyl)-1-piperazineethanesulfonic acid) at pH 7.4 (for Cm, Cf and Bk) or in 0.5% formic acid at pH 2 (for Ce, Th and Pu). Concentrations were 10 μM for ^{243}Am, ^{249}Bk and ^{249}Cf samples and 1 μM for Ce, ^{232}Th, ^{242}Pu and ^{248}Cm.

Protein fluorescence quenching binding assay. The affinity of Scn for complexes of **1** was quantified by monitoring the intrinsic fluorescence of the protein upon complex-binding, as described previously[38] and detailed in Supplementary Information.

Photophysics. UV–visible absorption spectra were recorded on an Ocean Optics USB 4000 absorption spectrometer, using quartz cells of 1.00 cm path length. Emission spectra were acquired on a HORIBA Jobin Yvon IBH FluoroLog-3 spectrofluorimeter, used in steady state mode. Luminescence lifetimes were determined on a HORIBA Jobin Yvon IBH FluoroLog-3 spectrofluorimeter, adapted for time-correlated single photon counting (TCSPC) and multichannel scaling (MCS) measurements. Further experiment and instrument details are provided in Supplementary Information.

Crystallography. For crystallization, 1 mM solutions of equimolar [Cf(III)**1**]$^-$ complex were mixed in a 2:1 molar ratio with Scn, which was then buffer-exchanged into 25 mM PIPES (pH = 7.0), 150 mM NaCl, 1 mM EDTA, and 0.01% w/w NaN_3, and concentrated to ~10 mg ml^{-1} protein. Diffraction-quality crystals were grown by vapour diffusion as detailed in Supplementary Information, along with data collection and refinement methods. Crystallographic statistics are reported in Supplementary Table 11.

Computational chemistry simulations. All calculations were performed with the latest development version of the open-source NWChem software suite[50]. Scalar relativistic density functional theory calculations were carried out with the B3LYP density functional[51,52], using the Stuttgart small-core effective core-potential and associated basis set for the actinide atoms[53] and all-electron DFT optimized valence double-ζ polarized (DZVP) basis sets[54] for the light atoms in the complex. UV–visible spectra were calculated at the time-dependent density functional theory (TDDFT) level of theory[55]. TDDFT equations were solved using a novel new symmetric Lanczos algorithm[56]. Geometries of solutions species were optimized within the COSMO model. The DIRAC code[57] and Dyall's relativistic triple-zeta basis set[58] were used to estimate the effect of atomic spin-orbit coupling on Bk(IV) with a $5f^7\ ^8S_{7/2}$ ground state, and Bk(III) with a $5f^8\ ^7F_6$ ground state at the Dirac–Hartree–Fock level of theory. For each atom an average-of-configurations SCF was performed followed by a Complete Active Space CI (COSCI) in the space covered by the $5f^7$ or $5f^8$ to project out all the states. Additional computational details are provided as Supplementary Information.

Data availability. The data supporting the findings discussed here are available within the paper and its Supplementary Information files, or from the corresponding authors upon request. The final models for the described protein structure have been deposited in the PDB[49], under accession code 5KIC.

Received 16 October 2016; accepted 2 March 2017; published online 10 April 2017

References

1. Kosyakov, V. N. Perspective methods for Berkelium–249 preparation and application. *J. Nucl. Sci. Technol.* **39,** 42–44 (2002).
2. Vértes, A., Nagy, S., Klencsár, Z. & Lovas, R. G. *Handbook of Nuclear Chemistry: Instrumentation, Separation Techniques Environmental Issues* (Kluwer Academic, 2003).
3. Hobart, D. E. & Peterson, J. R. in *The Chemistry of the Actinide and Transactinide Elements* (eds Morss, L. R., Edelstein, N., Fuger, J. & Katz, J. J.) Ch. 10, 1444–1498 (Springer, 2006).
4. Silver, M. A. *et al.* Characterization of berkelium(III) dipicolinate and borate compounds in solution and the solid state. *Science* **353,** aaf3762 (2016).
5. Hungate, F. P. *et al.* Preliminary data on ^{253}Es and ^{249}Bk metabolism in rats. *Health Phys.* **22,** 653–656 (1972).
6. Taylor, G. N. *et al.* Microscopic distribution of californium-249 and berkelium-249 in the soft tissues of beagles. *Health Phys.* **22,** 691–693 (1972).
7. Runde, W. H. & Mincher, B. J. Higher oxidation states of americium: preparation, characterization and use for separations. *Chem. Rev.* **111,** 5723–5741 (2011).
8. Czerwinski, K. R. *Studies of Fundamental Properties of Rutherfordium (Element 104) Using Organic Complexing Agents*. PhD thesis, Univ. California (1992).
9. Thompson, S. G., Ghiorso, A. & Seaborg, G. T. Element 97. *Phys. Rev.* **77,** 838–839 (1950).
10. Thompson, S. G., Cunningham, B. B. & Seaborg, G. T. Chemical properties of Berkelium. *J. Am. Chem. Soc.* **72,** 2798–2801 (1950).
11. Antonio, M. R., Williams, C. W. & Soderholm, L. Berkelium redox speciation. *Radiochim. Acta* **90,** 851–856 (2002).
12. Cotton, S. *Lanthanide and Actinide Chemistry* (Wiley, 2006).
13. Stokely, J. R., Baybarz, R. D. & Peterson, J. R. The formal potential of the Bk(IV)-Bk(III) couple in several media. *J. Inorg. Nucl. Chem.* **34,** 392–393 (1972).
14. Wadsworth, E., Duke, F. R. & Goetz, C. A. Present status of cerium (IV)–cerium (III) potentials. *Anal. Chem.* **29,** 1824–1825 (1957).
15. Gutmacher, R. G. *et al.* The absorption spectra of Bk^{3+} and Bk^{4+} in solution. *J. Inorg. Nucl. Chem.* **29,** 2341–2345 (1967).
16. Baybarz, R. D. & Stokely, J. R. Absorption spectra of Bk(III) and Bk(IV) in several media. *J. Inorg. Nucl. Chem.* **34,** 739–746 (1972).
17. Gutmacher, R. G., Bodé, D. D., Lougheed, R. W. & Hulet, E. K. The stability of tetravalent berkelium in acid solution and the absorption spectra of Bk(IV) and Bk(III). *J. Inorg. Nucl. Chem.* **35,** 979–994 (1973).
18. Milyukova, M. S., Malikov, D. A., Kuzovkina, E. V. & Myasoedov, B. F. Extraction of tetravalent berkelium by high molecular weight amines in the presence of heteropolyanions. *J. Radioanal. Nucl. Chem.* **104,** 81–89 (1986).
19. Payne, G. F. & Peterson, J. R. Possible stabilization of the tetravalent oxidation state of berkelium and californium in acetonitrile with triphenylarsine oxide. *Inorganica Chim. Acta* **139,** 111–112 (1987).
20. Morris, D. E., Hobart, D. E. & Palmer, P. D. Voltammetric investigation of the berkelium(IV/III) couple in concentrated aqueous carbonate solutions. *Radiochim. Acta* **49,** 125–134 (1990).
21. Bunin, D. I. *et al.* Dose-dependent efficacy and safety toxicology of hydroxypyridinonate actinide decorporation agents in rodents: towards a safe and effective human dosing regimen. *Radiat. Res.* **179,** 171–182 (2013).
22. Choi, T. A. *et al.* Biodistribution of the multidentate hydroxypyridinonate ligand [^{14}C]-3,4,3-LI(1,2-HOPO), a potent actinide decorporation agent. *Drug Dev. Res.* **76,** 107–122 (2015).
23. Choi, T. A. *et al. In vitro* metabolism and stability of the actinide chelating agent 3,4,3-LI(1,2-HOPO). *J. Pharm. Sci.* **104,** 1832–1838 (2015).
24. Sturzbecher-Hoehne, M., Deblonde, G. J. -P. & Abergel, R. J. Solution thermodynamic evaluation of hydroxypyridinonate chelators 3,4,3-LI(1,2-HOPO) and 5-LIO(Me-3,2-HOPO) for UO_2(VI) and Th(IV) decorporation. *Radiochim. Acta* **101,** 359–366 (2013).
25. Sturzbecher-Hoehne, M., Kullgren, B., Jarvis, E. E., An, D. D. & Abergel, R. J. Highly luminescent and stable hydroxypyridinonate complexes: a step towards new curium decontamination strategies. *Chem. Eur. J.* **20,** 9962–9968 (2014).
26. Sturzbecher-Hoehne, M., Choi, T. A. & Abergel, R. J. Hydroxypyridinonate complex stability of group (IV) metals and tetravalent f-block elements: the key to the next generation of chelating agents for radiopharmaceuticals. *Inorg. Chem.* **54,** 3462–3468 (2015).
27. Sturzbecher-Hoehne, M., Yang, P., D'Aléo, A. & Abergel, R. J. Intramolecular sensitization of americium luminescence in solution: shining light on short-lived forbidden 5f transitions. *Dalton Trans.* **45,** 9912–9919, (2016).
28. Deblonde, G. J.-P., Sturzbecher-Hoehne, M. & Abergel, R. J. Solution thermodynamic stability of complexes formed with the octadentate hydroxypyridinonate ligand 3,4,3-LI(1,2-HOPO): a critical feature for efficient chelation of lanthanide(IV) and actinide(IV) Ions. *Inorg. Chem.* **52,** 8805–8811 (2013).
29. Shannon, R. Revised effective ionic radii and systematic studies of interatomic distances in halides and chalcogenides. *Acta Crystallogr. A* **32,** 751–767 (1976).
30. Baybarz, R. D. Dissociation constants of the transplutonium element chelates of diethylenetriaminepenta-acetic acid (DTPA) and the application of DTPA chelates to solvent extraction separations of transplutonium elements from the lanthanide elements. *J. Inorg. Nucl. Chem.* **27,** 1831–1839 (1965).
31. Nugent, L. J. *et al.* Intramolecular energy transfer and sensitized luminescence in actinide (III) β-diketone chelates. *J. Phys. Chem.* **73,** 1540–1549 (1969).
32. Carnall, W., Beitz, J. & Crosswhite, H. Electronic energy level and intensity correlations in the spectra of the trivalent actinide aquo ions. III. Bk^{3+}. *J. Chem. Phys.* **80,** 2301–2308 (1984).
33. Barbanel, A. Nephelauxetic effect and hypersensitivity in the optical spectra of actinides. *Radiochim. Acta* **78,** 91–96 (1997).
34. Liu, G., Carnall, W., Jursich, G. & Williams, C. Analysis of the crystal-field spectra of the actinide tetrafluorides. II. AmF_4, CmF_4, Cm^{4+}:CeF_4, and Bk^{4+}:CeF_4. *J. Chem. Phys.* **101,** 8277–8289 (1994).
35. Carnall, W. T. *A Systematic Analysis of the Spectra of Trivalent Actinide Chlorides in D_{3h} Site Symmetry*. (Argonne National Laboratory, 1989).
36. Jursich, G. M. *et al.* Laser induced fluorescence of $^{249}Bk^{4+}$ in CeF_4. *Inorganica Chim. Acta* **139,** 273–274 (1987).
37. Nugent, L. J., Baybarz, R. D., Burnett, J. L. & Ryan, J. L. Electron-transfer and fd absorption bands of some lanthanide and actinide complexes and the standard (II-III) oxidation potential for each member of the lanthanide and actinide series. *J. Phys. Chem.* **77,** 1528–1539 (1973).
38. Allred, B. E. *et al.* Siderocalin-mediated recognition, sensitization, and cellular uptake of actinides. *Proc. Natl Acad. Sci. USA* **112,** 10342–10347 (2015).

39. Lundberg, D. & Persson, I. The size of actinoid (III) ions–structural analysis vs. common misinterpretations. *Coord. Chem. Rev.* **318,** 131–134 (2016).
40. Myasoedov, B. & Lebedev, I. Latest achievements in the analytical chemistry of actinides. *J. Radioanal. Nucl. Chem.* **147,** 5–26 (1991).
41. Maruyama, T. *et al.* Rapid chemical separation for Bk. *J. Nucl. Radiochem. Sci.* **3,** 155–158 (2002).
42. Peppard, D. F., Moline, S. W. & Mason, G. W. Isolation of berkelium by solvent extraction of the tetravalent species. *J. Inorg. Nucl. Chem.* **4,** 344–348 (1957).
43. Moore, F. L. New method for rapid separation of berkelium (IV) from cerium (IV) by anion exchange. *Anal. Chem.* **39,** 1874–1876 (1967).
44. Moore, F. L. Liquid–liquid extraction method for the separation of cerium (IV) from berkelium (IV) and other elements. *Anal. Chem.* **41,** 1658–1661 (1969).
45. Chudinov, E. G. & Pirozhkov, S. V. The separation of berkelium(III) from cerium(III). *J. Radioanal. Chem.* **10,** 41–46 (1972).
46. Liu, Y.-F. *et al.* Procedures for a fast separation of berkelium from complex mixtures of reaction products. *J. Radioanal. Nucl. Chem.* **76,** 119–124 (1983).
47. Chang, P. Y. *et al.* Analytical methods for the bioavailability evaluation of hydroxypyridinonate actinide decorporation agents in pre-clinical pharmacokinetic studies. *J. Chromatogr. Sep. Tech.* **4,** 196 (2013).
48. Goetz, D. H. *et al.* The neutrophil lipocalin NGAL is a bacteriostatic agent that interferes with siderophore-mediated iron acquisition. *Mol. Cell* **10,** 1033–1043 (2002).
49. Valiev, M. *et al.* NWChem: a comprehensive and scalable open-source solution for large scale molecular simulations. *Comput. Phys. Commun.* **181,** 1477–1489 (2010).
50. Becke, A. D. Density-functional exchange-energy approximation with correct asymptotic behavior. *Phys. Rev. A* **38,** 3098–3100 (1988).
51. Lee, C., Yang, W. & Parr, R. G. Development of the Colle-Salvetti correlation-energy formula into a functional of the electron density. *Phys. Rev. B* **37,** 785–789 (1988).
52. Küchle, W., Dolg, M., Stoll, H. & Preuss, H. Energy-adjusted pseudopotentials for the actinides. Parameter sets and test calculations for thorium and thorium monoxide. *J. Chem. Phys.* **100,** 7535–7542 (1994).
53. Godbout, N., Salahub, D. R., Andzelm, J. & Wimmer, E. Optimization of Gaussian-type basis sets for local spin density functional calculations. Part I. Boron through neon, optimization technique and validation. *Can. J. Chem.* **70,** 560–571 (1992).
54. Runge, E. & Gross, E. K. Density-functional theory for time-dependent systems. *Phys. Rev. Lett.* **52,** 997–1000 (1984).
55. Brabec, J. *et al.* Efficient algorithms for estimating the absorption spectrum within linear response TDDFT. *J. Chem. Theory Comput.* **11,** 5197–5208 (2015).
56. Jensen, H. J. Aa. *et al.* DIRAC12. http://www.diracprogram.org (2012)
57. Dyall, K. G. Relativistic double-zeta, triple-zeta, and quadruple-zeta basis sets for the actinides Ac–Lr. *Theor. Chem. Acc.* **117,** 491–500 (2007).
58. Berman, H. M. *et al.* The Protein Data Bank. *Nucleic Acids Res.* **28,** 235–242 (2000).

Acknowledgements

This work was supported by the US Department of Energy (DoE), Office of Science Early Career Research Program and Office of Science, Office of Basic Energy Sciences, Chemical Sciences, Geosciences, and Biosciences Division at the Lawrence Berkeley National Laboratory under contract DE-AC02-05CH11231 (R.J.A.), by the National Institutes of Health (R01DK073462, R.K.S.), and by the Scientific Discovery through Advanced Computing (SciDAC) program of the US DoE, Office of Science, Office of Advanced Scientific Computing and Office of Basic Energy Sciences (W.A.d.J.). The Radiochemical Engineering and Development Center at Oak Ridge National Laboratory is supported by the US DoE, Isotope Development and Production for Research and Applications Program. The Advanced Light Source (ALS) and Energy Research Scientific Computing Center (NERSC) are supported by the Director, Office of Science, and Office of Basic Energy Sciences, of the US DoE under contract no. DE-AC02-05CH11231. The Innovative and Novel Computational Impact on Theory and Experiment (INCITE) program provided an award of computer time through the Oak Ridge Leadership Computing Facility, a US DoE Office of Science User Facility supported under Contract DE-AC05-00OR22725. We thank M. Allaire, S. Morton, J. Bramble, K. Engle, M. Dupray, and I. Tadesse for assistance in implementing diffraction data collection on radioactive crystals at ALS 5.0.2 beamline.

Author contributions

G.J.-P.D., M.S.-H., W.A.d.J., R.K.S., and R.J.A. designed the research. G.J.-P.D., M.S.-H., and M.-C.I. collected and analysed optical spectroscopy and mass spectrometry data. R.J.A. and D. D. A crystallized the protein–metal adducts. P.B.R., D.D.A., and C.Y.R. collected and analysed crystallographic data. P.B.R. and R.K.S. solved the structures. J.B. and W.A.d.J. performed theoretical computations. All of the authors discussed the results and commented on the manuscript.

Additional information

Supplementary information and chemical compound information are available in the online version of the paper. Reprints and permissions information is available online at www.nature.com/reprints. Publisher's note: Springer Nature remains neutral with regard to jurisdictional claims in published maps and institutional affiliations. Correspondence and requests for materials should be addressed to W.A.d.J., R.K.S. and R.J.A.

Competing financial interests

The authors declare no competing financial interests.

nature chemistry

SUPPLEMENTARY INFORMATION

DOI: 10.1038/NCHEM.2759

In the format provided by the authors and unedited.

Chelation and stabilization of berkelium in oxidation state +IV

Gauthier J-P. Deblonde[1], Manuel Sturzbecher-Hoehne[1], Peter B. Rupert,[2] Dahlia D. An,[1] Marie-Claire Illy,[1] Corie Y. Ralston,[3] Jiri Brabec,[4] Wibe A. de Jong[*,5] Roland K. Strong[*,2] and Rebecca J. Abergel[*1]

[1] *Chemical Sciences Division, Lawrence Berkeley National Laboratory, Berkeley, California 94720, USA*

[2] *Division of Basic Science, Fred Hutchinson Cancer Research Center, Seattle, WA 98109, USA*

[3] *Berkeley Center for Structural Biology, Lawrence Berkeley National Laboratory, Berkeley, CA 94720, USA*

[4] *J. Heyrovsky Institute of Physical Chemistry, 18223 Prague 8, Czech Republic*

[5] *Computational Research Division, Lawrence Berkeley National Laboratory, Berkeley, CA 94720, USA*

* e-mail: rjabergel@lbl.gov; rstrong@fhcrc.org; wadejong@lbl.gov

Supplementary Information

Table of Contents

A. Materials and Methods

Caution: ^{249}Cf (half-life of 351 years; specific activity: 4.1 Ci.g^{-1}) represents a serious health risk owing to its α emission (6.194 MeV) and, more importantly, its γ emission (0.388 MeV), as well as the emission of its decay products. ^{249}Cf decays to ^{245}Cm (half-life of 8,500 years), which is an α emitter (5.623 MeV) and undergoes spontaneous fission i.e. emitting a large flux of neutrons. ^{249}Bk (half-life of 330 days) is a β emitter that decays to ^{249}Cf therefore representing a serious health risk too. ^{248}Cm (half-life of 3.49x10^5 years; 5.162 MeV) and ^{242}Pu (half-life of 3.74x10^5 years; 4.985 MeV) are α emitters and represent serious health risks. All these radioactive elements where manipulated in laboratories specially designed for the safe handling of transuranium elements.

1. Materials

Chemicals were acquired from commercial suppliers and were used as received. The ligand 3,4,3-LI(1,2-HOPO) (**1**) was prepared and characterized as previously described (*1*). Stock solutions (4 mM) of **1** were prepared by direct dissolution of a weighed portion of ligand in DMSO and aliquots were removed prior to each set of experiments. Aliquots of acidified stocks of carrier-free ^{249}Cf and ^{248}Cm (95.78% ^{248}Cm, 4.12% ^{246}Cm, 0.06% ^{245}Cm, 0.02% ^{244}Cm/^{247}Cm isotopic distribution by atom percentage) from the Lawrence Berkeley National Laboratory were used in this work. A stock solution of ^{249}Bk(III) in 0.1 M HCl was prepared from solid $^{249}BkCl_3$ obtained from the Oak Ridge National Laboratory. All measurements reported here were completed within six weeks of the original separation work and within two weeks of dissolution of the dry salt. All aqueous solutions were prepared using deionized water purified by a Millipore Milli-Q reverse osmosis cartridge system and the pH was adjusted as needed with concentrated HCl or KOH. The pH of solutions was measured with a conventional pH meter at 25°C (Metrohm Brinkmann) that was equipped with a glass electrode (Micro Combi, Metrohm) filled with KCl and calibrated with pH standards. For direct spectroscopic measurements, equimolar amounts of metal and chelator were used to constitute complex solutions (40 μM, pH 8.4) in 0.1 M CHES buffer. Recombinant human Scn was prepared as previously described (*2*).

2. Liquid Chromatography - Mass Spectrometry

The experimental setting used for liquid chromatography-high resolution mass spectrometry assays (LC-HRMS) has been previously described (*3*). LC-HRMS spectra were acquired on a UPLC Waters Xevo system interfaced with a QTOF mass spectrometer (Waters Corporation, Milford, MA, USA) in Micromass Z-spray geometry. Chromatographic separation was achieved on an analytical Zorbax Eclipse column (Agilent Technologies, XDB-C18, 5 μm, 4.6 × 150 mm) maintained at ambient temperature (25 °C) with two mobile phases (water (A) and methanol (B)) containing 0.5% formic acid (pH = 3.4). Samples (10 μL injection) were eluted using a gradient initially held constant at 7% B for 6.0 min and were then progressed to 40% B in the next 6.0 min and held at 40% B for 10 min. Mobile phase B was then increased to 99% over 3.0 min, held constant at 99% for 5.0 min, and then

rapidly switched to 7% B and held until 46 min for equilibration. The flow rate was maintained at 0.5 mL/min. The mass spectrometer equipped with an ESI source was operated in positive ion mode, and mass spectra were acquired in the continuum mode across the m/z range of 100−1200, at 5 s per scan, with a 14 ms interscan delay. Data acquisition and instrument control were accomplished using MassLynx software, version 4.1. Samples were infused into the ionization chamber from the LC system. The operating parameters were as follows: the nebulization gas flow rate was set to 600 L/h with a desolvation temperature of 375 °C, the cone gas flow rate was set to 30 L/h, and the ion source temperature was 125 °C. The capillary, sampling cone, and extraction cone voltages were tuned to 2.7 kV, 47 V, and 3.3 V, respectively. Liquid nitrogen served as nebulizer and argon was used as collision gas with collision energies up to 50 eV. A calibration check of the instrument was performed with 0.5 mM sodium formate, prior to sample analysis. Samples containing an equal concentration of actinide and **1** were prepared in 0.1 M HEPES buffer at pH 7.4 (for Cm, Cf and Bk) or in 0.5% formic acid at pH 2 (for Ce, Th, and Pu). The concentrations used were 10 μM for ^{243}Am, ^{249}Bk and ^{249}Cf samples and 1 μM for Ce, ^{232}Th, ^{242}Pu, and ^{248}Cm. For consistency, an addition of 0.1 μM of [Zr^{IV}**1**] was performed in each sample in order to use the Zr complex as internal reference. The retention times of independent samples were then normalized using that of [Zr^{IV}**1**].

3. Protein Fluorescence Quenching Binding Assay

The affinity of siderocalin for an apo- or holo-siderophore can be quantified by monitoring the intrinsic fluorescence of the protein upon siderophore-binding (*4*). The intrinsic fluorescence in proteins is generally attributed to tryptophan residues, with some emissions due to tyrosine and phenylalanine; two residues W31 and W79 are found in the proximity of the siderocalin binding site (*5*). 400 μL of a siderocalin solution (50 nM) containing 5 % DMSO in TBS buffer (pH 7.4) were incrementally perturbed by successive additions of 2.5 μL of a titrant solution containing 4 μM of ^{249}Bk and **1** in TBS buffer (pH 7.4). Similar incremental titrations were performed with ^{249}Cf. Fluorescence quenching of Scn was measured after each titrant addition, with 3-nm slit band pass, using the characteristic wavelengths λ_{ex} = 280 nm and λ_{em} = 320–360 nm. Fluorescence values were corrected for dilution upon addition of titrant. Fluorescence data were analyzed by nonlinear regression analysis of fluorescence response versus ligand concentration using a one-site binding model in the program HypSpec (*6*). The entire procedure (titration and fitting) was performed in duplicate.

4. Photophysics

UV-visible absorption spectra were recorded either on a Ocean Optics USB 4000 absorption spectrometer, using quartz cells of 1.00 cm path length. Emission spectra were acquired on a HORIBA Jobin Yvon IBH FluoroLog-3 spectrofluorimeter, used in steady state mode. Spectra were reference corrected for both the excitation light source variation (lamp and grating) and the emission spectral response (detector and grating). Luminescence lifetimes were determined on a HORIBA

Jobin Yvon IBH FluoroLog-3 spectrofluorimeter, adapted for time-correlated single photon counting (TCSPC) and multichannel scaling (MCS) measurements, using a sub-microsecond Xenon flashlamp (Jobin Yvon, 5000XeF) as the lightsource, with an input pulse energy (100 nF discharge capacitance) of ca. 50 mJ, yielding an optical pulse duration of less than 300 ns at full width at half maximum (FWHM). Spectral selection was achieved by passage through a double grating excitation monochromator (2.1 nm/mm dispersion, 1200 grooves/mm). Emission was monitored perpendicular to the excitation pulse, again with spectra selection. A thermoelectrically cooled single photon detection module (HORIBA Jobin Yvon IBH, TBX-04- D) incorporating fast rise time photo-multiplier tubes (PMT), wide bandwidth preamplifier, and picosecond constant fraction discriminator, was used as the detector. Signals were acquired using an IBH DataStation Hub photon counting module and data analysis was performed using the commercially available DAS 6 decay analysis software package from HORIBA Jobin Yvon IBH. Goodness of fit was assessed by minimizing the reduced chi squared function, and visual inspection of the weighted residuals. Each trace contained at least 5000 points, and the estimated error on the reported lifetime values is ±10%. Quantum yields were determined using the previously described optical dilution method with quinine sulfate as a standard (*7*).

5. Crystallography

For crystallization, 1 mM solutions of equimolar $[Cf^{III}\mathbf{1}]^-$ complex were mixed in a 2:1 molar ratio with Scn, which was then buffer-exchanged into 25 mM PIPES (pH = 7.0), 150 mM NaCl, 1 mM EDTA, and 0.01% w/w NaN_3, and concentrated to ~10 mg/ml protein. Diffraction-quality crystals were grown by vapor diffusion from drops containing 1 µl of the ternary metal-chelator-protein complex plus 1 µl of well solution (50 mM NaCl, 200 mM Li_2SO_4, 100 mM NaOAc (pH = 4.3-4.5), 1.2-1.4 M $(NH_4)_2SO_4$). Crystals were cryo-preserved by transfer to 50 mM NaCl, 200 mM Li_2SO_4, 100 mM NaOAc (pH=4.3-4.5), 1.2 M $(NH_4)_2SO_4$, and 20% v/v glycerol. Diffraction data were collected on beamline 5.0.2 at the Advanced Light Source (ALS, Berkeley, CA). Diffraction data were integrated and scaled with HKL-2000 (*8*). Initial phases were determined by rigid body positional refinement with Refmac (*9*) using 3FW5.pdb as a starting structure, or molecular replacement with MolRep (*10*) using 3FW5.pdb as a search model. Structures were refined through iterative rounds of positional refinement using Refmac (*9*) alternating with model building using COOT (*11*), followed by a final round of TLS refinement (*12*). Residues or side-chains that did not exhibit clear electron density in $2F_{obs}$-F_{calc} Fourier syntheses when contoured at 0.7σ were removed or truncated to the Cβ atom. The quality of the final model was assessed using ProCheck (*13*) and Molprobity (*14*). Crystallographic statistics are reported in Supplementary Table 11. Final models have been deposited in the PDB (*15*).

6. Computational Chemistry Simulations

All the computational chemistry calculations in the manuscript were performed with the latest development version of the open-source NWChem software suite (*16*). Scalar relativistic density functional theory calculations were carried out with the B3LYP (*17*, *18*) density functional, using the Stuttgart small-core effective core-potential and associated basis set for the actinide atoms (*19*) and all-electron DFT optimized valence double-ζ polarized (DZVP) basis sets (*20*) for the light atoms in the complex. The geometries of the complexes were optimized, followed by frequency calculations to ensure the calculated structure had no imaginary frequencies and was in a minimum energy configuration. Both the coordinates and frequencies of the calculated species are listed in Tables S2-S5. To validate the computational approach, additional geometry optimizations with and all-electron DFT optimized valence triple-ζ polarized (TZVP) basis sets on the light elements were done. All calculated TZVP structures were found to be very similar to those obtained with DZVP and the latter structures were used for the subsequent UV-visible, solvation and redox potential calculations.

The UV-visible spectra were calculated at the time-dependent density functional theory (TDDFT) level of theory (*21*). Because of the large number of individual states involved in each calculated spectrum the TDDFT equations were solved using a novel new symmetric Lanczos algorithm developed by Brabec and coworkers (*22*). For each of the three polarization directions 1400 Lanczos steps were performed. All the obtained Ritz values were Gaussian broadened and all three polarizations were summed to form the final calculated spectrum.

The electrochemical reduction potential relative to a normal hydrogen electrode (NHE) we follow the approach outlined by Hay and coworkers (*23*). The various Gibbs free energies at room temperature of the overall reaction

$$Bk(\mathbf{1})^{4+} + ½\ H_2 + H_2O \rightarrow Bk(\mathbf{1})^{3+} + H_3O^+ \qquad \text{(SR1)}$$

were calculated. The electrochemical reduction potential is the negative of the calculated free energy of reaction SR1. For the solution phase the COSMO model (*24*) was utilized, and the dielectric constant was set to 78.0. All geometries of the solutions species were optimized within the COSMO model and verified to be minima via frequency calculations. Calculated coordinates and frequencies for the solvated berkelium species are listed in Tables S6 and S7. Energies for the hydrogen electrode were calculated analogous those for the berkelium solution species. Tables S2 and S3 list the contributions to all the calculated energies for the berkelium species in the gas-phase and solution phase respectively. The Bk^{4+}/Bk^{3+} electrochemical potential relative to NHE in solution is calculated from SR1 and Table S3 is -0.13 V.

Spin-orbit coupling is expected to influence the reaction free energies and elec. The DIRAC code (*25*) and Dyall's relativistic triple-zeta basis set (*26*) were used to estimate the effect of atomic spin-orbit coupling on Bk^{4+} with a $5f^7\ ^8S_{7/2}$ ground state, and Bk^{3+} with a $5f^8\ ^7F_6$ ground state at the Dirac-

Hartree-Fock level of theory. For each atom an average-of-configurations SCF was performed followed by a Complete Active Space CI (COSCI) in the space covered by the $5f^7$ or $5f^8$ to project out all the states. The spin-orbit coupling is found to increase the Gibbs free energy difference +0.47 eV, a value very similar to the 0.49 eV obtained by Cao and Dolg (*27*).

The use of DFT with the B3LYP functional has been shown to overestimate the fourth ionization potential (*23*), leading to an electrochemical potential that is too high. Determining how much the ionization potential is overestimated by the computational method used is challenging given there is no experimental data available for Bk, with the exception of the first IP. Cao and Dolg (*27*) have attempted to accurately determine the fourth IPs for the actinide series, and this data was used as the reference. Fourth IP values for the atoms U-Bk were calculated using DFT and B3LYP with a consistent set of Stuttgart small-core effective core-potentials and associated basis sets (*19*). The DFT results for the U-Bk series were found to overestimate the fourth IP by an average of 0.67 eV (or a -0.67 V contribution to the electrochemical potential), with the later actinides (including Bk) showing deviations that are larger than the average.

Considering the spin-orbit coupling of +0.47 V and the overestimate of the ionization potential by DFT with B3LYP of at least -0.67 V, the calculated electrochemical potential of -0.13 V is likely to be an upper bound.

B. Supplementary Figures and Tables

Supplementary Table 1
Stability constants for complexes of **1**.

Species	$\log \beta_{mlh}$	Reference	Species	$\log \beta_{mlh}$	Reference
$[Zr^{IV}\mathbf{1}]$	43.1	(*3*)	$[U^{VI}O_2\mathbf{1}]^{2-}$	18.0	(*28*)
			$[U^{VI}O_2\mathbf{1}H]^{-}$	22.0	
			$[U^{VI}O_2\mathbf{1}H_2]$	24.6	
			$[U^{VI}O_2\mathbf{1}(OH)]^{3-}$	8.6	
$[Ce^{IV}\mathbf{1}]$	41.5	(*29*)	$[Ce^{III}\mathbf{1}]^{-}$	17.4	(*29*)
			$[Ce^{III}\mathbf{1}H]$	21.2	
			$[Ce^{III}\mathbf{1}(OH)]^{2-}$	8.3	
$[Th^{IV}\mathbf{1}]$	40.1	(*29*)	$[Am^{III}\mathbf{1}]^{-}$	20.4	(*30*)
$[Pu^{IV}\mathbf{1}]$	43.5	(*3*)	$[Cm^{III}\mathbf{1}]^{-}$	21.8	(*7*)

Supplementary Table 2
Calculated energies of the gas-phase Bk^{3+} and Bk^{4+} species.

Calculated property	**Bk^{3+}**	**Bk^{4+}**	
Total energy in Hartree	-3342.210477	-3342.087434	
Zero-point energy in Hartree	0.679392	0.682195	
Thermal correction to enthalpy in Hartree	0.728653	0.730694	
Total entropy in cal/mol-K	276.442	268.059	

Supplementary Table 3
Calculated energies used in the determination of the Bk^{3+}-Bk^{4+} electrochemical reduction potential versus a normal hydrogen electrode (NHE).

Calculated property	**Bk^{3+}**	**Bk^{4+}**	
Total energy in Hartree	-3342.335255	-3342.154650	
Zero-point energy in Hartree	0.678413	0.680609	
Thermal correction to enthalpy in Hartree	0.727940	0.729433	
Total entropy in cal/mol-K	277.650	271.473	
Calculated property	**H_3O^+**	**H_2O**	**H_2**
Total energy in Hartree	-76.824985	-76.434066	-1.149051
Zero-point energy in Hartree	0.034797	0.021039	0.010124
Thermal correction to enthalpy in Hartree	0.038603	0.024817	0.013427
Total entropy in cal/mol-K	48.293	46.508	32.487

Supplementary Table 4

Calculated geometry and vibrational modes for Bk^{3+}. The units for the Cartesian coordinates are in Angstrom while the vibrational modes and infra-red intensities are in cm^{-1} and $(Debye/Angstrom)^2$ respectively.

Cartesian coordinates					Vibrational Modes	
Atom	**X-coord**	**Y-coord**	**Z-coord**		**Frequency**	**Intensity**
C	-1.1979	1.9211	-2.8708		7.395	0.002
C	-0.6216	2.4121	-4.0371		20.372	0.007
C	0.4409	1.7100	-4.6284		28.028	0.003
C	0.8875	0.5203	-4.0763		30.648	0.018
C	0.2970	-0.0056	-2.8953		40.444	0.008
N	-0.7336	0.7649	-2.3248		42.966	0.031
H	0.9073	2.0962	-5.5321		49.279	0.124
H	-1.0359	3.3103	-4.4801		55.265	0.029
H	1.6985	-0.0533	-4.5135		57.242	0.022
O	-1.2778	0.2733	-1.2079		71.292	0.039
O	0.6095	-1.0794	-2.3071		72.105	0.007
C	-2.4443	2.6044	-2.3356		81.129	0.02
O	-3.3544	2.8176	-3.1486		85.407	0.008
N	-2.5286	3.0323	-1.0424		90.068	0.039
C	-1.4553	2.9752	-0.0424		93.474	0.057
H	-1.9403	2.8279	0.9283		100.311	0.086
H	-0.8589	2.0803	-0.1986		101.808	0.054
C	4.3454	-1.2672	-1.1764		112.593	0.138
C	5.1768	-2.2115	-1.7684		114.173	0.017
C	4.7687	-3.5499	-1.8523		122.779	0.048
C	3.5272	-3.9280	-1.3692		124.991	0.044
C	2.6537	-2.9782	-0.7787		127.91	0.131
N	3.1412	-1.6671	-0.6618		137.494	0.408
H	5.4217	-4.2887	-2.3122		143.482	0.104
H	6.1231	-1.8587	-2.1593		150.105	0.303
H	3.1609	-4.9476	-1.4358		151.411	0.095
O	2.3341	-0.8167	-0.0142		166.769	0.65
O	1.4864	-3.2225	-0.3441		171.987	1.064
C	4.8218	0.1773	-1.1824		175.411	1.268
O	5.9400	0.4329	-1.6573		176.867	0.291
N	3.9857	1.1326	-0.7158		182.28	0.359
H	3.1343	0.7996	-0.2572		192.707	0.225
C	4.4001	2.5322	-0.7266		198.432	0.045
H	5.1477	2.7067	0.0558		207.832	0.039
H	4.8991	2.7038	-1.6851		211.698	0.089
C	2.0560	1.0879	3.1445		217.066	0.023
C	2.5364	0.8375	4.4247		222.552	0.019
C	2.0770	-0.2868	5.1268		225.755	0.251
C	1.2261	-1.1865	4.5071		230.785	0.029
C	0.7847	-0.9782	3.1727		238.243	0.176
N	1.1269	0.2564	2.5883		244.399	0.154
H	2.4272	-0.4767	6.1390		248.322	0.22
H	3.3047	1.4896	4.8237		274.294	0.221
H	0.8992	-2.1032	4.9874		290.273	0.378
O	0.5504	0.5447	1.4152		301.371	0.186
O	0.1147	-1.7957	2.4776		309.552	0.124
C	2.7585	2.1365	2.3053		310.923	0.138

O	3.9912	2.0653	2.2571		314.668	0.275
N	2.0567	3.1128	1.6508		319.822	0.045
C	2.8688	4.0333	0.8370		330.891	0.265
H	2.3042	4.9587	0.7249		335.579	0.089
H	3.7875	4.2757	1.3838		339.18	0.082
C	-4.6719	-1.7410	0.5602		339.821	0.094
C	-5.5779	-2.7635	0.3023		358.517	0.148
C	-5.1139	-4.0252	-0.0937		391.711	0.165
C	-3.7556	-4.2439	-0.2547		394.948	0.093
C	-2.8147	-3.2118	-0.0065		396.439	0.077
N	-3.3287	-1.9918	0.4596		408.511	0.038
H	-5.8219	-4.8265	-0.2937		422.772	0.08
H	-6.6303	-2.5289	0.4031		428.729	0.23
H	-3.3534	-5.1959	-0.5863		432.733	0.013
O	-2.4191	-1.0745	0.7943		445.18	0.037
O	-1.5582	-3.3050	-0.1682		453.184	0.194
C	-5.2387	-0.3667	0.8680		461.945	0.584
O	-6.4503	-0.2616	1.1110		472.035	0.279
N	-4.3934	0.6912	0.7865		481.537	0.266
H	-3.4043	0.4654	0.6500		485.747	1.581
C	-4.8665	2.0540	0.9831		495.72	0.143
H	-4.2195	2.5509	1.7184		498.876	0.034
H	-5.8581	1.9674	1.4314		508.296	0.023
C	3.2361	3.5328	-0.5791		509.728	0.006
H	2.3438	3.1405	-1.0799		510.582	0.039
H	3.5268	4.4330	-1.1368		514.715	0.096
C	0.7201	3.4856	2.1766		520.491	0.011
H	0.1249	2.5704	2.2009		526.899	0.005
H	0.8349	3.8403	3.2112		528.688	0.004
C	-0.0669	4.5681	1.4234		533.124	0.006
H	0.4895	5.5126	1.4071		534.726	0.04
H	-0.9405	4.7649	2.0609		576.61	0.127
C	-0.5826	4.2478	0.0096		579.784	0.146
H	0.2446	4.1535	-0.7017		584.019	0.239
H	-1.1756	5.1083	-0.3249		593.387	0.295
C	-3.7491	3.7670	-0.6737		625.825	0.695
H	-4.0273	4.4089	-1.5146		628.654	0.406
H	-3.4924	4.4180	0.1701		631.976	0.308
C	-4.9702	2.9057	-0.3047		644.155	0.228
H	-5.2325	2.2620	-1.1485		647.527	0.238
H	-5.8053	3.6083	-0.1758		651.465	0.151
Bk	-0.0719	-1.4214	0.0803		653.195	0.221
					656.777	0.758
					682.004	0.534
					689.914	1.288
					699.273	0.804
					704.913	1.746
					724.712	0.259
					729.63	0.065
					730.185	0.316
					730.641	0.256
					743.754	0.468
					746.811	1.174
					757.581	0.599
					760.815	0.868

					764.137	0.539
					777.569	0.08
					786.293	0.368
					792.367	0.604
					793.253	0.486
					798.592	0.054
					804.614	0.603
					806.832	0.721
					809.95	0.053
					834.96	0.731
					839.252	0.25
					840.259	0.415
					844.935	0.106
					845.703	0.349
					850.639	0.028
					861.936	0.187
					875.966	0.004
					876.985	0.011
					878.051	0.04
					885.566	0.148
					901.839	0.371
					924.819	0.308
					931.713	0.218
					946.481	0.582
					946.769	0.195
					954.196	0.04
					957.286	0.005
					963.235	0.013
					964.137	0.014
					965.155	0.129
					1001.372	0.272
					1008.871	0.172
					1013.314	0.019
					1015.378	0.332
					1053.162	0.048
					1071.461	0.037
					1079.443	0.052
					1083.972	0.159
					1085.81	0.226
					1087.961	0.162
					1090.139	0.199
					1090.968	0.111
					1101.924	0.19
					1105.107	0.214
					1111.13	0.218
					1117.986	0.101
					1126.387	0.167
					1162.368	1.311
					1163.322	0.713
					1164.451	1.34
					1165.351	0.551
					1177.224	3.201
					1182.496	4.966
					1184.395	2.685
					1199.076	6.053

					1206.241	1.073
					1206.7	0.243
					1210.825	2.339
					1220.591	1.812
					1225.379	1.9
					1226.111	0.465
					1250.311	0.568
					1255.042	0.183
					1255.488	0.105
					1258.662	0.068
					1262.454	0.024
					1265.458	0.459
					1268.346	0.303
					1273.362	0.444
					1293.752	1.887
					1304.476	3.471
					1318.198	0.862
					1319.358	1.954
					1323.68	2.341
					1344.057	1
					1347.222	1.207
					1350.255	0.398
					1362.643	0.605
					1379.391	2.066
					1388.554	0.018
					1392.471	1.82
					1401.238	0.171
					1403.537	0.234
					1410.568	0.36
					1413.965	0.914
					1416.937	1.749
					1417.886	0.915
					1420.047	0.401
					1420.143	0.696
					1423.737	0.445
					1439.349	1.081
					1442.39	0.195
					1442.541	0.129
					1447.787	0.47
					1451.991	1.895
					1459.097	0.304
					1472.935	2.159
					1483.051	0.023
					1486.624	0.188
					1490.837	0.364
					1495.016	1.345
					1498.358	0.574
					1511.075	0.06
					1514.615	0.281
					1516.257	0.642
					1519.924	0.392
					1536.801	0.139
					1548.059	6.35
					1561.485	6.515
					1572.728	3.906

					1576.369	5.685
					1580.618	2.546
					1586.423	7.196
					1592.384	0.65
					1593.374	1.087
					1594.11	1.253
					1594.879	0.256
					1656.736	22.13
					1661.382	5.136
					1666.453	18.744
					1677.466	6.108
					1684.034	7.88
					1698.489	8.065
					1708.013	3.001
					1711.112	5.501
					3005.31	0.742
					3029.617	1.001
					3032.922	1.1
					3033.754	0.529
					3035.246	1.14
					3044.019	0.259
					3052.74	1.342
					3057.485	0.961
					3058.376	0.079
					3071.626	1.04
					3072.407	0.733
					3096.413	1.605
					3101.088	0.747
					3104.928	0.447
					3112.855	0.377
					3124.029	0.167
					3127.762	0.445
					3135.891	0.272
					3151.866	0.575
					3184.009	0.65
					3186.646	0.506
					3187.568	0.611
					3188.206	0.531
					3194.953	0.233
					3223.113	0.143
					3224.495	0.172
					3224.874	0.152
					3225.964	0.085
					3235.118	0.059
					3236.543	0.044
					3249.538	0.037
					3250.154	0.045
					3418.577	6.372
					3427.301	4.591

Supplementary Table 5

Calculated geometry and vibrational modes for Bk^{4+}. The units for the Cartesian coordinates are in Angstrom while the vibrational modes and infra-red intensities are in cm^{-1} and $(Debye/Angstrom)^2$ respectively.

Cartesian coordinates				Vibrational Modes	
Atom	**X-coord**	**Y-coord**	**Z-coord**	**Frequency**	**Intensity**
C	-1.1776	1.8384	-2.8562	20.003	0.016
C	-0.6422	2.2567	-4.0654	24.299	0.013
C	0.3686	1.4979	-4.6797	30.967	0.018
C	0.8074	0.3149	-4.1081	40.399	0.001
C	0.2572	-0.1269	-2.8821	42.274	0.06
N	-0.7017	0.6923	-2.2961	49.217	0.001
H	0.7948	1.8326	-5.6218	51.674	0.161
H	-1.0526	3.1449	-4.5310	55.004	0.009
H	1.5694	-0.3065	-4.5663	67.402	0.011
O	-1.1969	0.2478	-1.1259	74.213	0.037
O	0.5532	-1.1961	-2.2498	78.865	0.034
C	-2.4110	2.5479	-2.3130	84.916	0.018
O	-3.3303	2.7118	-3.1223	96.002	0.022
N	-2.4751	3.0253	-1.0386	96.924	0.049
C	-1.3991	3.0009	-0.0405	98.111	0.087
H	-1.8784	2.8279	0.9288	103.76	0.105
H	-0.7668	2.1335	-0.2028	107.934	0.017
C	4.2643	-1.2081	-1.1967	122.924	0.049
C	5.0962	-2.1684	-1.7539	124.41	0.017
C	4.6976	-3.5134	-1.7966	129.219	0.019
C	3.4598	-3.8897	-1.3047	135.203	0.075
C	2.5976	-2.9195	-0.7474	138.655	0.048
N	3.0626	-1.6139	-0.6813	149.695	0.242
H	5.3583	-4.2589	-2.2316	152.434	0.105
H	6.0431	-1.8262	-2.1530	162.927	0.05
H	3.1002	-4.9126	-1.3374	171.24	0.097
O	2.2296	-0.7548	-0.0583	180.035	0.009
O	1.4199	-3.1419	-0.2909	186.714	0.291
C	4.7410	0.2405	-1.2348	193.836	0.03
O	5.8418	0.4737	-1.7459	202.205	0.815
N	3.9274	1.2068	-0.7495	204.995	0.952
H	3.1046	0.9003	-0.2370	207.071	0.232
C	4.3785	2.5982	-0.7273	209.893	1.012
H	5.1471	2.7276	0.0431	213.803	0.067
H	4.8597	2.7863	-1.6908	218.733	0.116
C	1.9321	1.0563	3.1237	227.728	0.018
C	2.3701	0.8012	4.4134	229.383	0.003
C	1.9298	-0.3543	5.0820	237.012	0.289
C	1.1472	-1.2843	4.4199	243.165	0.335
C	0.7480	-1.0534	3.0816	246.532	0.076
N	1.0508	0.1933	2.5396	251.604	0.242
H	2.2532	-0.5456	6.1018	254.766	0.239
H	3.1001	1.4693	4.8556	282.316	0.37
H	0.8505	-2.2254	4.8704	291.684	0.389
O	0.4775	0.4771	1.3518	303.591	0.157
O	0.1394	-1.8788	2.3227	309.683	0.105
C	2.6642	2.0853	2.2779	312.445	0.26

O	3.8819	1.9144	2.1810		317.17	0.305
N	2.0116	3.1194	1.6724		325.713	0.187
C	2.8772	4.0471	0.9153		334.668	0.292
H	2.3546	5.0011	0.8556		337.174	0.013
H	3.7972	4.2151	1.4859		340.819	0.076
C	-4.5355	-1.7032	0.6114		342.798	0.129
C	-5.4362	-2.7204	0.3304		354.845	0.095
C	-4.9778	-3.9595	-0.1417		390.494	0.177
C	-3.6247	-4.1620	-0.3580		393.399	0.187
C	-2.7028	-3.1320	-0.0744		398.347	0.056
N	-3.1980	-1.9531	0.4608		406.284	0.075
H	-5.6879	-4.7527	-0.3596		419.423	0.06
H	-6.4877	-2.5019	0.4719		425.113	0.24
H	-3.2249	-5.0906	-0.7514		436.606	0.002
O	-2.2684	-1.0582	0.8288		440.95	0.039
O	-1.4332	-3.1900	-0.2675		446.195	0.069
C	-5.1006	-0.3399	0.9788		471.852	0.632
O	-6.2913	-0.2694	1.2972		484.096	1.087
N	-4.2850	0.7366	0.8404		490.4	0.678
H	-3.3021	0.5524	0.6478		492.27	0.029
C	-4.7881	2.0943	1.0264		498.682	0.968
H	-4.1533	2.6135	1.7561		504.31	2.298
H	-5.7751	1.9881	1.4788		508.129	0.02
C	3.2414	3.6176	-0.5247		510.791	0.054
H	2.3431	3.2810	-1.0549		514.091	0.02
H	3.5608	4.5392	-1.0270		519.548	0.261
C	0.7003	3.5460	2.2194		526.7	0.068
H	0.0809	2.6501	2.2941		533.223	0.069
H	0.8479	3.9296	3.2388		535.9	0.102
C	-0.0745	4.6240	1.4466		536.495	0.076
H	0.4858	5.5650	1.4323		540.644	0.065
H	-0.9549	4.8290	2.0710		568.065	0.208
C	-0.5665	4.2985	0.0255		575.18	0.241
H	0.2709	4.2332	-0.6769		585.853	0.208
H	-1.1777	5.1444	-0.3102		594.845	0.464
C	-3.6979	3.7711	-0.6819		624.242	0.576
H	-3.9826	4.3854	-1.5401		628.291	0.778
H	-3.4330	4.4485	0.1369		629.72	0.555
C	-4.9131	2.9211	-0.2735		637.231	0.567
H	-5.1999	2.2651	-1.0998		643.034	0.311
H	-5.7402	3.6302	-0.1385		646.883	0.861
Bk	-0.0469	-1.3980	0.0468		648.905	0.456
					653.494	0.317
					655.472	1.025
					659.793	1.078
					686.093	0.602
					704.465	0.186
					727.046	0.53
					729.259	0.136
					730.349	0.05
					730.498	0.097
					745.963	0.227
					752.388	0.593
					758.989	0.612
					760.542	0.596

					766.961	0.931
					773.918	0.082
					786.841	0.443
					796.566	1.05
					797.456	0.552
					803.266	0.054
					809.61	0.382
					812.142	0.344
					815.014	0.617
					838.13	0.574
					840.577	0.396
					844.09	0.186
					847.17	0.489
					857.863	0.169
					863.309	0.21
					872.354	0.059
					874.774	0.038
					881.807	0.097
					898.29	0.208
					901.344	0.011
					904.888	0.009
					923.986	0.167
					930.608	0.246
					943.687	0.371
					945.627	0.065
					966.577	0.13
					973.827	0.096
					978.465	0.04
					985.206	0.028
					988.742	0.004
					1003.609	0.198
					1012.355	0.022
					1017.19	0.207
					1019.532	0.198
					1051.827	0.038
					1074.219	0.169
					1081.452	0.116
					1086.816	0.168
					1089.804	0.267
					1090.28	0.155
					1091.335	0.163
					1091.86	0.062
					1102.514	0.24
					1104.976	0.093
					1109.479	0.267
					1118.71	0.113
					1129.322	0.132
					1169.061	0.573
					1170.017	0.054
					1170.206	0.088
					1174.782	0.428
					1185.713	1.323
					1188.929	2.438
					1193.95	1.023
					1204.352	1.833

					1207.538	0.923
					1212.19	0.54
					1223.958	2.69
					1225.927	1.962
					1231.837	2.279
					1233.599	0.778
					1255.991	0.126
					1261.54	0.255
					1265.501	0.102
					1266.229	0.692
					1266.741	0.373
					1268.652	0.65
					1270.216	0.234
					1274.891	0.529
					1290.845	0.933
					1294.474	3.305
					1317.91	1.264
					1320.762	1.115
					1325.336	2.204
					1345.06	0.934
					1345.728	0.291
					1348.398	1.029
					1360.773	0.703
					1380.25	0.774
					1386.602	0.007
					1394.073	1.588
					1399.93	0.281
					1402.982	0.312
					1405.659	5.046
					1408.059	0.961
					1410.361	0.734
					1411.26	0.491
					1414.287	0.348
					1415.754	0.521
					1424.968	0.399
					1433.204	0.041
					1435.214	1.455
					1436.183	0.27
					1442.751	0.273
					1448.525	0.582
					1453.413	2.974
					1472.942	2.328
					1480.528	0.013
					1485.651	0.15
					1489.218	0.342
					1493.263	1.337
					1500.268	0.29
					1507.842	0.049
					1513.409	0.261
					1513.949	0.447
					1517.803	0.367
					1529.041	0.31
					1532.98	8.765
					1542.079	2.508
					1554.628	5.959

					1560.831	1.93
					1562.808	7.552
					1581.551	5.594
					1595.804	0.322
					1597.183	0.322
					1598.08	0.048
					1598.721	0.696
					1652.456	13.571
					1654.244	3.498
					1657.513	11.192
					1664.893	2.409
					1696.355	8.435
					1708.736	6.72
					1725.96	7.859
					1728.613	5.309
					3019.973	0.552
					3040.948	0.612
					3043.853	0.704
					3045.922	0.261
					3050.952	0.659
					3056.28	0.064
					3067.086	0.469
					3068.777	0.309
					3071.555	0.163
					3078.352	0.528
					3088.419	0.423
					3103.384	1.289
					3108.621	0.597
					3121.773	0.222
					3125.042	0.293
					3135.543	0.29
					3136.263	0.372
					3151.021	0.056
					3162.771	0.4
					3207.479	0.304
					3209.19	0.126
					3209.595	0.287
					3210.706	0.03
					3214.262	0.24
					3237.57	0.018
					3238.036	0.01
					3238.409	0.007
					3239.087	0.002
					3243.7	0.063
					3249.351	0.081
					3254.187	0.109
					3255.465	0.129
					3515.78	5.432
					3532.873	4.186

Supplementary Table 6

Calculated geometry and vibrational modes for Bk^{3+} in solution using the COSMO solvation model. The units for the Cartesian coordinates are in Angstrom while the vibrational modes and infra-red intensities are in cm^{-1} and $(Debye/Angstrom)^2$ respectively.

Cartesian coordinates					Vibrational Modes	
Atom	**X-coord**	**Y-coord**	**Z-coord**		**Frequency**	**Intensity**
C	-1.3359	1.8987	-2.7489		15.413	0.005
C	-0.7661	2.4805	-3.8716		19.985	0.015
C	0.3064	1.8328	-4.5092		25.407	0.05
C	0.7734	0.6177	-4.0329		27.371	0.058
C	0.1956	0.0193	-2.8850		34.904	0.02
N	-0.8583	0.7114	-2.2889		40.565	0.19
H	0.7663	2.2854	-5.3839		46.376	0.089
H	-1.1597	3.4217	-4.2395		52.416	0.088
H	1.5947	0.0930	-4.5115		57.922	0.043
O	-1.4181	0.1355	-1.2092		66.345	0.182
O	0.5503	-1.0831	-2.3404		71.973	0.06
C	-2.6006	2.4909	-2.1514		78.08	0.3
O	-3.5898	2.5468	-2.9124		81.61	0.088
N	-2.6167	2.9907	-0.8988		86.81	0.139
C	-1.4659	2.9882	0.0267		88.979	0.148
H	-1.8869	2.9369	1.0336		93.465	0.143
H	-0.8995	2.0704	-0.1130		95.593	0.327
C	4.4484	-1.3264	-1.0501		105.731	0.165
C	5.3046	-2.2994	-1.5496		110.939	0.18
C	4.8935	-3.6402	-1.5998		117.463	0.46
C	3.6234	-3.9898	-1.1730		121.767	1.008
C	2.7339	-3.0094	-0.6700		133.984	0.598
N	3.2121	-1.7031	-0.5883		135.858	1.216
H	5.5653	-4.4014	-1.9877		141.675	0.029
H	6.2778	-1.9842	-1.9042		151.711	0.461
H	3.2639	-5.0132	-1.2171		159.201	2.23
O	2.3822	-0.8171	-0.0106		160.812	1.906
O	1.5303	-3.2314	-0.2814		162.903	0.933
C	4.9145	0.1192	-1.0939		166.233	0.576
O	6.0990	0.3466	-1.4232		175.842	0.446
N	4.0325	1.0971	-0.8314		186.754	0.059
H	3.1098	0.8049	-0.5074		194.71	0.211
C	4.4000	2.5122	-0.9503		196.863	0.229
H	5.2251	2.7339	-0.2650		204.679	0.162
H	4.7807	2.6693	-1.9654		208.836	0.07
C	1.9512	1.1687	3.1258		216.986	0.126
C	2.3678	0.9991	4.4377		222.244	0.025
C	1.9108	-0.1115	5.1673		228.975	0.124
C	1.1350	-1.0777	4.5450		233.152	0.21
C	0.7469	-0.9304	3.1904		238.418	0.579
N	1.0680	0.2830	2.5781		239.722	0.573
H	2.2115	-0.2401	6.2037		245.348	0.316
H	3.0703	1.7056	4.8670		267.711	0.624
H	0.8281	-1.9837	5.0584		281.338	1.071
O	0.5182	0.5297	1.3750		298.399	0.639

O	0.1307	-1.8014	2.4815		301.48	0.338
C	2.7045	2.1113	2.2012		310.22	0.249
O	3.9133	1.8416	2.0622		314.385	0.746
N	2.1050	3.1494	1.5803		322.515	0.257
C	2.9752	3.9922	0.7307		326.077	0.44
H	2.4994	4.9682	0.6607		330.868	0.032
H	3.9316	4.1384	1.2428		339.567	0.17
C	-4.6356	-1.7192	0.3960		342.834	0.117
C	-5.5340	-2.6748	-0.0606		368.545	0.259
C	-5.0706	-3.9026	-0.5569		376.429	0.416
C	-3.7095	-4.1460	-0.6258		393.873	0.066
C	-2.7788	-3.1767	-0.1805		395.648	0.297
N	-3.2921	-2.0080	0.3816		403.958	0.204
H	-5.7779	-4.6509	-0.9044		416.556	0.17
H	-6.5882	-2.4292	-0.0394		426.856	0.266
H	-3.3084	-5.0705	-1.0294		429.941	0.12
O	-2.3854	-1.1708	0.9134		440.739	0.183
O	-1.5028	-3.2945	-0.2523		456.942	1.506
C	-5.1908	-0.3663	0.8059		459.211	0.324
O	-6.4288	-0.2338	0.8896		468.39	0.382
N	-4.3250	0.6470	0.9978		474.838	0.389
H	-3.3333	0.4054	0.9733		482.012	2.625
C	-4.7675	2.0124	1.2880		493.815	0.291
H	-4.0184	2.4695	1.9398		496.648	0.089
H	-5.6950	1.9414	1.8596		506.599	0.086
C	3.2289	3.4816	-0.7082		507.581	0.112
H	2.3069	3.0679	-1.1309		511.487	0.091
H	3.4562	4.3764	-1.2976		517.42	0.039
C	0.8129	3.6629	2.1172		521.554	0.243
H	0.1829	2.7939	2.3128		525.857	0.019
H	1.0153	4.1456	3.0816		528.226	0.048
C	0.0316	4.6759	1.2671		530.509	0.079
H	0.6244	5.5836	1.1165		535.978	0.009
H	-0.7998	4.9800	1.9158		573.929	0.555
C	-0.5624	4.2337	-0.0826		575.266	0.459
H	0.2222	4.0565	-0.8245		586.167	0.48
H	-1.1566	5.0746	-0.4580		596.218	0.86
C	-3.8262	3.7266	-0.4705		618.667	1.65
H	-4.1710	4.3303	-1.3143		624.584	0.893
H	-3.5140	4.4143	0.3192		628.009	0.542
C	-5.0097	2.8802	0.0314		644.987	0.328
H	-5.3936	2.2494	-0.7757		645.933	1.25
H	-5.8027	3.6001	0.2675		650.598	0.576
Bk	-0.0432	-1.4059	0.0589		651.909	0.774
					655.644	1.72
					661.493	4.424
					682.809	1.735
					695.886	3.878
					697.935	0.315
					727.782	1.225
					728.562	0.216
					730.812	0.361
					734.698	0.697
					748.174	1.496
					749.854	1.192

754.048	1.383
758.211	1.165
759.054	1.411
774.619	0.256
784.369	0.684
792.548	2.375
793.47	2.033
798.772	0.177
804.029	0.451
806.966	1.104
809.888	1.12
830.551	1.522
834.908	1.236
837.828	0.698
839.119	1.057
856.897	0.123
859.058	0.931
869.638	0.095
876.116	0.197
883.333	0.107
889.328	0.01
890.626	0
897.519	0.453
914.328	0.946
920.955	0.737
938.4	1.106
940.338	0.216
956.187	0.362
980.102	0.03
980.244	0.022
980.433	0.017
988.657	0.028
999.179	0.706
1003.891	0.202
1005.605	0.317
1014.428	0.433
1050.725	0.214
1062.718	0.193
1074.194	0.271
1079.785	0.139
1085.143	0.549
1087.002	0.396
1088.107	0.252
1089.668	0.425
1096.988	0.703
1099.487	0.405
1101.685	0.383
1109.234	0.292
1129.591	0.104
1158.364	1.642
1160.311	0.58
1161.588	0.392
1162.369	1.289
1176.786	11.8
1178.155	3.997

					1179.789	3.956
					1195.798	6.557
					1198.47	6.91
					1202.318	2.349
					1216.174	3.169
					1221.342	3.302
					1224.547	2.318
					1225.918	1.149
					1244.342	0.233
					1248.333	0.247
					1249.659	0.425
					1251.251	0.676
					1252.53	0.469
					1260.121	0.348
					1263.778	0.17
					1272.768	0.54
					1294.025	1.542
					1295.096	4.084
					1312.838	0.579
					1313.05	2.873
					1331.768	1.777
					1340.187	1.54
					1341.29	1.393
					1346.007	2.192
					1361.616	0.465
					1384.775	2.373
					1388	0.298
					1390.317	3.599
					1396.95	10.068
					1398.989	3.273
					1400.347	4.31
					1400.873	1.443
					1404.181	1.775
					1405.631	3.826
					1406.979	0.287
					1411.536	0.517
					1428.365	2.62
					1431.105	1.338
					1433.024	0.109
					1433.333	0.034
					1437.101	1.752
					1450.107	1.559
					1461.233	5.739
					1468.553	1.969
					1472.12	0.268
					1477.621	3.523
					1483.374	1.825
					1488.589	2.589
					1492.239	0.352
					1498.005	3.964
					1500.196	1.115
					1504.412	2.532
					1506.816	1.211
					1522.207	23.873
					1527.98	4.471

					1533.766	13.774
					1539.216	13.529
					1545.955	7.543
					1557.613	13.116
					1562	13.257
					1586.763	1.88
					1587.891	0.917
					1588.712	0.616
					1593.558	2.106
					1626.479	39.361
					1629.949	17.889
					1633.937	26.829
					1638.96	10.617
					1647.306	6.384
					1650.35	14.339
					1665.881	1.826
					1670.703	4.235
					3039.577	0.391
					3052.068	1.89
					3054.931	0.666
					3056.449	0.778
					3060.512	0.439
					3063.115	1.366
					3080.264	0.614
					3082.025	1.334
					3091.294	0.383
					3096.491	0.772
					3103.141	1.047
					3107.573	0.561
					3111.622	2.335
					3115.753	1.045
					3118.075	1.37
					3139.1	0.746
					3143.186	0.867
					3152.368	0.575
					3172.734	0.531
					3191.931	0.188
					3210.546	0.126
					3210.599	0.157
					3210.736	0.169
					3211.83	0.1
					3227.687	0.073
					3228.775	0.052
					3229.279	0.093
					3231.564	0.065
					3233.763	0.026
					3239.456	0.005
					3254.686	0.037
					3256.715	0.046
					3451.102	10.557
					3460.415	9.45

Supplementary Table 7

Calculated geometry and vibrational modes for Bk^{4+} in solution using the COSMO solvation model. The units for the Cartesian coordinates are in Angstrom while the vibrational modes and infra-red intensities are in cm^{-1} and $(Debye/Angstrom)^2$ respectively.

Cartesian coordinates					Vibrational Modes	
Atom	**X-coord**	**Y-coord**	**Z-coord**		**Frequency**	**Intensity**
C	-1.2692	1.8865	-2.7013		18.353	0.009
C	-0.7067	2.4210	-3.8492		23.455	0.016
C	0.3596	1.7494	-4.4739		27.721	0.069
C	0.8310	0.5474	-3.9680		30.999	0.06
C	0.2556	0.0020	-2.8000		38.295	0.146
N	-0.7717	0.7194	-2.2131		43.855	0.155
H	0.8105	2.1732	-5.3671		47.601	0.029
H	-1.1040	3.3460	-4.2519		57.264	0.175
H	1.6433	0.0025	-4.4381		60.36	0.091
O	-1.3045	0.1742	-1.0989		72.217	0.246
O	0.5880	-1.0955	-2.2132		74.084	0.132
C	-2.5439	2.4805	-2.1219		85.283	0.12
O	-3.5212	2.5073	-2.8977		87.937	0.052
N	-2.5804	2.9955	-0.8774		90.912	0.082
C	-1.4414	3.0353	0.0616		94.262	0.162
H	-1.8711	2.9679	1.0634		100.699	0.312
H	-0.8346	2.1432	-0.0693		105.018	0.056
C	4.3347	-1.3476	-1.0030		114.719	0.323
C	5.1796	-2.3354	-1.4864		119.303	0.035
C	4.7548	-3.6741	-1.5274		128.015	0.092
C	3.4787	-4.0123	-1.1105		134.843	0.469
C	2.6087	-3.0116	-0.6256		139.409	0.272
N	3.0977	-1.7211	-0.5471		147.276	0.985
H	5.4231	-4.4434	-1.9044		148.892	0.17
H	6.1577	-2.0355	-1.8411		166.189	0.344
H	3.1058	-5.0307	-1.1497		170.814	0.026
O	2.2655	-0.8318	0.0346		175.134	0.432
O	1.3900	-3.1956	-0.2425		187.421	1.221
C	4.8062	0.0970	-1.0631		188.465	2.423
O	6.0021	0.3067	-1.3519		190.131	2.381
N	3.9172	1.0841	-0.8697		194.867	0.872
H	2.9800	0.8229	-0.5715		196.648	1.336
C	4.2988	2.4948	-1.0070		205.157	0.268
H	5.1422	2.7068	-0.3421		207.634	0.383
H	4.6565	2.6430	-2.0320		219.182	0.158
C	1.9009	1.1495	3.0808		223.734	0.089
C	2.3051	0.9591	4.3913		229.792	0.015
C	1.8656	-0.1756	5.0972		236.952	0.1
C	1.1174	-1.1508	4.4564		242.059	0.292
C	0.7359	-0.9724	3.1079		244.201	1.149
N	1.0385	0.2490	2.5234		250.06	0.26
H	2.1654	-0.3156	6.1320		251.32	0.231
H	2.9924	1.6676	4.8415		277.036	1.316
H	0.8291	-2.0742	4.9480		285.61	1.205
O	0.4693	0.4910	1.3221		299.897	0.439

O	0.1313	-1.8285	2.3610		306.321	0.326
C	2.6570	2.1012	2.1636		310.258	0.527
O	3.8564	1.8085	2.0073		316.994	0.822
N	2.0630	3.1549	1.5678		324.424	0.403
C	2.9294	3.9882	0.7041		329.294	0.408
H	2.4659	4.9706	0.6468		335.116	0.034
H	3.8974	4.1187	1.1979		342.159	0.118
C	-4.5237	-1.7300	0.4226		345.038	0.232
C	-5.4121	-2.6920	-0.0350		364.544	0.211
C	-4.9403	-3.8909	-0.5934		377.714	0.525
C	-3.5787	-4.1011	-0.7273		390.448	0.154
C	-2.6687	-3.1241	-0.2721		398.103	0.272
N	-3.1800	-1.9988	0.3487		405.177	0.397
H	-5.6447	-4.6416	-0.9409		416.94	0.135
H	-6.4703	-2.4728	0.0306		426.314	0.234
H	-3.1704	-4.9974	-1.1830		433.777	0.167
O	-2.2601	-1.1772	0.8922		443.514	0.241
O	-1.3832	-3.1938	-0.3789		455.096	0.337
C	-5.0884	-0.3950	0.8776		470.279	1.299
O	-6.3231	-0.2973	1.0142		480.797	2.951
N	-4.2395	0.6372	1.0393		488.756	1.645
H	-3.2435	0.4430	0.9532		492.94	0.014
C	-4.7085	1.9974	1.3159		495.452	4.621
H	-3.9674	2.4785	1.9591		500.22	1.204
H	-5.6303	1.9133	1.8936		505.289	0.408
C	3.1446	3.4768	-0.7406		513.787	0.058
H	2.2090	3.0735	-1.1430		516.168	0.055
H	3.3693	4.3691	-1.3346		519.171	0.237
C	0.7977	3.6934	2.1429		531.31	0.192
H	0.1523	2.8392	2.3550		533.399	0.206
H	1.0375	4.1651	3.1039		537.507	0.253
C	0.0194	4.7293	1.3178		539.995	0.14
H	0.6185	5.6349	1.1811		543.161	0.093
H	-0.8050	5.0264	1.9784		566.6	0.991
C	-0.5866	4.3133	-0.0346		569.288	0.845
H	0.1863	4.1832	-0.7980		588.97	0.443
H	-1.2160	5.1446	-0.3714		599.695	0.926
C	-3.8117	3.7078	-0.4691		620.155	0.969
H	-4.1683	4.2844	-1.3263		620.874	3.853
H	-3.5216	4.4189	0.3077		630.021	1.422
C	-4.9729	2.8388	0.0455		632.71	0.676
H	-5.3390	2.1853	-0.7519		647.541	1.863
H	-5.7849	3.5410	0.2692		647.599	0.606
Bk	-0.0330	-1.3696	0.0529		649.172	3.172
					652.514	0.686
					656.14	0.639
					659.319	2.692
					683.509	1.091
					700.984	0.398
					728.561	0.388
					729.481	1.433
					733.843	0.461
					734.581	0.321
					750.762	1.534
					750.973	1.195

					753.899	0.826
					758.856	1.815
					760.408	1.803
					774.911	0.214
					785.591	0.89
					796.144	2.734
					799.75	1.469
					804.328	0.344
					808.989	1.03
					810.159	1.274
					815.382	1.182
					834.263	1.328
					840.275	0.454
					840.578	1.34
					841.817	0.908
					859.714	0.886
					865.435	0.165
					873.806	0.189
					881.886	0.207
					889.189	0.057
					894.237	0.023
					898.259	0.255
					905.39	0.026
					914.416	0.87
					920.6	0.761
					940.001	0.75
					942.644	0.34
					958.362	0.347
					985.906	0.02
					991.493	0.03
					998.298	0.023
					1001.972	0.091
					1002.212	0.695
					1009.247	0.519
					1010.447	0.503
					1017.118	0.255
					1052.179	0.184
					1063.802	0.397
					1074.263	0.381
					1079.607	0.223
					1084.298	0.404
					1087.495	0.623
					1087.628	0.4
					1089.278	0.285
					1096.372	0.568
					1099.994	0.827
					1102.525	0.317
					1108.821	0.264
					1130.17	0.113
					1160.592	0.533
					1161.053	0.378
					1164.804	0.198
					1166.872	0.665
					1180.626	2.498
					1189.765	5.135

1190.863	2.846
1196.705	0.739
1203.048	4.45
1207.656	1.18
1223.684	3.21
1225.208	3.711
1227.924	2.377
1233.788	1.134
1251.452	0.236
1257.762	0.331
1260.444	1.167
1264.649	1.358
1265.748	0.22
1266.901	0.661
1267.072	1.348
1275.731	0.694
1294.382	1.526
1296.57	2.753
1313.631	3.117
1316.483	0.799
1334.452	1.729
1340.09	1.459
1341.645	1.511
1344.365	2.216
1359.889	0.467
1384.098	7.306
1384.538	7.287
1386.478	1.291
1389.507	8.016
1392.543	1.706
1396.699	4.414
1398.559	4.519
1400.842	0.976
1404.239	0.824
1408.225	0.063
1411.762	0.343
1426.1	2.872
1429.037	1.332
1430.916	0.829
1433.443	0.048
1433.995	0.065
1444.425	2.339
1460.534	6.309
1468.593	1.534
1473.905	0.273
1476.557	4.567
1483.922	1.185
1490.257	2.592
1495.721	0.296
1500.013	2.937
1502.99	0.951
1505.03	0.832
1508.473	1.484
1515.414	21.632
1519.717	1.542

					1529.077	10.774
					1531.601	8.543
					1544.986	2.735
					1560.163	11.309
					1564.448	13.254
					1588.593	1.161
					1591.062	0.477
					1592.814	0.28
					1598.27	1.423
					1630.859	37.221
					1633.668	12.221
					1636.036	26.72
					1641.365	8.68
					1651.143	6.73
					1657.812	16.002
					1671.196	3.042
					1673.443	6.42
					3042.636	0.306
					3053.964	1.86
					3056.266	0.588
					3058.386	0.789
					3062.792	0.397
					3065.629	1.445
					3082.432	0.617
					3085.507	1.194
					3096.435	0.303
					3097.854	0.509
					3107.723	0.843
					3110.473	0.873
					3114.661	1.408
					3118.189	0.698
					3119.285	2.163
					3131.861	1.059
					3146.953	0.814
					3159.748	0.409
					3175.899	0.502
					3201.135	0.204
					3218.394	0.154
					3218.531	0.095
					3219.386	0.056
					3219.701	0.1
					3235.463	0.006
					3238.051	0.003
					3238.348	0.009
					3240.427	0.006
					3240.491	0.001
					3245.993	0.004
					3256.822	0.077
					3259.027	0.065
					3503.359	10.273
					3518.612	8.989

Supplementary Table 8

Calculated geometry and vibrational modes for Pu^{4+}. The units for the Cartesian coordinates are in Angstrom while the vibrational modes and infra-red intensities are in cm^{-1} and $(Debye/Angstrom)^2$ respectively.

Cartesian coordinates					Vibrational Modes	
Atom	**X-coord**	**Y-coord**	**Z-coord**		**Frequency**	**Intensity**
C	-1.4689	1.7951	-2.6371		20.31	0.004
C	-1.0281	2.2368	-3.8751		26.158	0.023
C	0.0106	1.5507	-4.5287		30.021	0.009
C	0.5794	0.4245	-3.9583		31.505	0.034
C	0.1269	-0.0388	-2.6997		42.026	0.061
N	-0.8872	0.6917	-2.0925		45.881	0.024
H	0.3613	1.9014	-5.4959		48.161	0.047
H	-1.5234	3.0890	-4.3251		54.594	0.092
H	1.3751	-0.1346	-4.4388		60.716	0.042
O	-1.3039	0.2158	-0.9027		73.87	0.02
O	0.5615	-1.0527	-2.0581		74.555	0.069
C	-2.6919	2.4468	-2.0096		84.251	0.02
O	-3.6862	2.5480	-2.7353		90.481	0.053
N	-2.6598	2.9540	-0.7448		95.05	0.047
C	-1.4818	3.0109	0.1337		95.718	0.049
H	-1.8701	3.0278	1.1571		100.341	0.051
H	-0.9194	2.0847	0.0544		103.967	0.053
C	4.2898	-1.4367	-1.0569		117.479	0.038
C	5.0946	-2.4411	-1.5737		124.693	0.002
C	4.6649	-3.7779	-1.5465		127.773	0.039
C	3.4215	-4.1027	-1.0326		128.438	0.061
C	2.5839	-3.0865	-0.5186		139.402	0.038
N	3.0885	-1.7948	-0.5075		147.434	0.17
H	5.3052	-4.5580	-1.9501		152.655	0.039
H	6.0428	-2.1406	-2.0024		164.081	0.029
H	3.0377	-5.1173	-1.0190		167.954	0.06
O	2.2864	-0.8950	0.0974		179.667	0.028
O	1.3986	-3.2456	-0.0604		188.601	0.187
C	4.7834	0.0005	-1.1862		192.292	0.335
O	5.8881	0.1879	-1.7080		197.569	0.534
N	3.9769	1.0083	-0.7767		203.55	0.88
H	3.1518	0.7508	-0.2413		205.125	0.317
C	4.4401	2.3930	-0.8728		211.465	0.371
H	5.2207	2.5757	-0.1259		214.323	0.511
H	4.9115	2.4960	-1.8538		219.502	0.39
C	2.0023	1.2896	3.1376		225.976	0.089
C	2.3964	1.1471	4.4577		227.238	0.447
C	1.8855	0.0824	5.2213		237.588	0.025
C	1.0651	-0.8677	4.6363		240.809	0.045
C	0.7068	-0.7507	3.2728		244.959	0.06
N	1.1063	0.4052	2.6155		251.764	0.411

H	2.1768	-0.0229	6.2630		255.114	0.327
H	3.1390	1.8283	4.8573		283.191	0.42
H	0.7058	-1.7394	5.1726		291.269	0.246
O	0.6000	0.5768	1.3756		297.109	0.306
O	0.0567	-1.6058	2.5794		309.965	0.088
C	2.7647	2.2076	2.1976		312.796	0.445
O	3.9684	1.9678	2.0834		325.829	0.098
N	2.1390	3.2170	1.5248		328.665	0.345
C	3.0176	4.0299	0.6592		332.245	0.15
H	2.5293	4.9938	0.5199		336.844	0.037
H	3.9602	4.2154	1.1862		342.061	0.126
C	-4.4873	-1.7950	0.1851		343.673	0.162
C	-5.3490	-2.6473	-0.4870		356.356	0.051
C	-4.8397	-3.7443	-1.2020		386.418	0.226
C	-3.4742	-3.9580	-1.2685		390.51	0.237
C	-2.5881	-3.0914	-0.5874		396.992	0.039
N	-3.1489	-2.0775	0.1735		403.717	0.087
H	-5.5198	-4.4095	-1.7274		416.462	0.129
H	-6.4057	-2.4110	-0.4554		420.296	0.202
H	-3.0336	-4.7697	-1.8375		435.309	0.013
O	-2.2705	-1.3883	0.9296		442.448	0.064
O	-1.3087	-3.1647	-0.5998		456.315	0.075
C	-5.0732	-0.5328	0.7955		471.983	0.453
O	-6.2899	-0.4834	0.9967		482.535	1.478
N	-4.2340	0.5169	0.9819		488.395	0.918
H	-3.2409	0.3590	0.8370		492.911	0.064
C	-4.7444	1.8278	1.3723		498.087	1.635
H	-4.0348	2.2784	2.0761		501.438	1.216
H	-5.6738	1.6499	1.9166		509.676	0.167
C	3.3194	3.4439	-0.7400		512.122	0.023
H	2.3957	3.0687	-1.1953		515.539	0.003
H	3.6290	4.3014	-1.3501		520.652	0.228
C	0.8783	3.7651	2.0808		528.707	0.037
H	0.2419	2.9133	2.3287		533.445	0.061
H	1.1039	4.2846	3.0233		535.391	0.162
C	0.0763	4.7497	1.2145		538.954	0.037
H	0.6724	5.6420	0.9961		541.958	0.074
H	-0.7268	5.1027	1.8759		561.314	1.157
C	-0.5725	4.2395	-0.0845		570.161	0.301
H	0.1878	4.0077	-0.8382		593.103	0.265
H	-1.1692	5.0628	-0.4949		600.425	0.629
C	-3.8743	3.6650	-0.2958		601.338	0.25
H	-4.2385	4.2802	-1.1236		625.729	0.98
H	-3.5656	4.3415	0.5080		629.424	0.726
C	-5.0342	2.7774	0.1881		632.908	0.455
H	-5.4262	2.1955	-0.6497		637.821	0.638
H	-5.8347	3.4650	0.4910		648.881	0.616
Pu	-0.0207	-1.3880	0.2349		651.196	0.254
					655.475	0.275
					656.235	0.845
					661.689	0.979
					685.683	0.623
					703.162	0.216
					732.541	0.025
					733.445	0.279

					733.977	0.068
					734.349	0.374
					750.356	0.362
					754.91	0.712
					760.037	0.474
					762.146	0.874
					764.722	0.955
					779.253	0.094
					785.705	0.399
					800.002	1.263
					801.471	0.889
					805.359	0.04
					813.092	0.121
					815.791	0.738
					818.392	0.888
					839.199	0.61
					842.501	0.396
					844.854	0.192
					845.311	0.74
					861.319	0.142
					868.746	0.122
					874.808	0.018
					877.588	0.068
					884.861	0.056
					897.789	0.238
					901.332	0.022
					906.695	0.011
					922.975	0.307
					931.483	0.242
					942.957	0.22
					946.966	0.094
					963.066	0.139
					978.379	0.01
					980.617	0.004
					987.178	0.01
					989.605	0.011
					1005.759	0.191
					1014.085	0.015
					1014.824	0.119
					1023.234	0.19
					1054.594	0.059
					1069.026	0.087
					1079.408	0.122
					1082.272	0.186
					1085.62	0.306
					1088.515	0.192
					1089.808	0.117
					1090.83	0.074
					1097.362	0.2
					1104.815	0.159
					1111.977	0.308
					1115.816	0.106
					1129.736	0.129
					1169.87	0.37
					1170.962	0.138

1171.755	0.092
1175.278	0.342
1185.809	1.194
1191.446	2.559
1195.217	1.484
1203.986	1.222
1208.335	1.369
1214.41	0.882
1224.733	3.752
1228.451	1.528
1233.012	1.948
1235.211	0.525
1257.265	0.052
1263.472	0.31
1266.564	0.665
1267.454	0.256
1268.181	0.465
1268.886	0.257
1272.837	0.368
1277.871	0.661
1290.215	1.485
1298.375	2.005
1317.22	1.126
1321.641	0.639
1325.645	3.007
1346.147	0.031
1346.961	0.596
1349.447	1.736
1365.447	0.554
1384.084	1.191
1394.354	0.134
1396.314	1.245
1402.405	0.225
1405.545	0.237
1407.623	3.937
1410.444	1.429
1412.972	0.782
1414.865	0.567
1417.553	0.221
1418.355	0.39
1424.821	0.639
1436.149	0.798
1439.654	0.265
1442.155	0.417
1446.897	0.71
1453.973	1.345
1455.518	2.002
1469.55	2.077
1482.395	0.014
1488.867	0.078
1490.061	0.585
1494.695	0.298
1496.975	1.276
1508.712	0.052
1512.165	0.238

					1515.074	0.421
					1518.901	0.573
					1536.892	7.905
					1539.762	0.929
					1546.675	3.388
					1558.668	7.639
					1564.075	1.647
					1567.126	8.976
					1578.516	6.398
					1598.659	0.1
					1599.572	0.893
					1600.595	0.045
					1601.988	0.926
					1653.017	13.519
					1656.419	3.642
					1660.362	12.441
					1667.434	3.476
					1699.382	8.52
					1712.842	7.667
					1724.407	5.197
					1729.588	6.745
					3011.546	0.64
					3036.978	0.821
					3042.518	0.311
					3045.696	0.723
					3049.808	0.207
					3056.073	0.665
					3059.746	0.687
					3062.213	0.417
					3065.736	0.189
					3075.154	0.899
					3084.961	0.407
					3096.671	1.474
					3100.849	0.84
					3115.637	0.295
					3116.826	0.236
					3128.343	0.509
					3133.301	0.414
					3140.136	0.169
					3156.108	0.463
					3192.687	0.124
					3201.843	0.284
					3202.924	0.189
					3204.49	0.298
					3204.716	0.172
					3232.773	0.004
					3233.218	0.029
					3233.456	0.032
					3234.217	0.005
					3235.296	0.005
					3242.105	0.01
					3250.453	0.118
					3250.532	0.136
					3532.107	4.188
					3554.582	4.04

Supplementary Table 9

Calculated geometry and vibrational modes for Am^{3+}. The units for the Cartesian coordinates are in Angstrom while the vibrational modes and infra-red intensities are in cm^{-1} and $(Debye/Angstrom)^2$ respectively.

Cartesian coordinates					Vibrational Modes	
Atom	X-coord	Y-coord	Z-coord		Frequency	Intensity
C	-1.3200	1.9303	-2.7820		14.446	0.003
C	-0.7961	2.4212	-3.9726		19.861	0.005
C	0.2555	1.7320	-4.5975		27.207	0.004
C	0.7421	0.5550	-4.0526		30.286	0.018
C	0.2046	0.0298	-2.8466		38.682	0.009
N	-0.8182	0.7852	-2.2448		41.949	0.025
H	0.6813	2.1178	-5.5212		48.312	0.102
H	-1.2412	3.3095	-4.4054		53.734	0.038
H	1.5454	-0.0095	-4.5151		56.074	0.017
O	-1.3216	0.2905	-1.1093		70.399	0.033
O	0.5603	-1.0343	-2.2637		74.082	0.019
C	-2.5541	2.5993	-2.2029		80.945	0.026
O	-3.4991	2.7950	-2.9794		84.222	0.01
N	-2.5899	3.0324	-0.9096		88.294	0.022
C	-1.4657	3.0048	0.0349		91.838	0.044
H	-1.9043	2.9240	1.0349		95.96	0.08
H	-0.8989	2.0871	-0.1016		96.782	0.095
C	4.3716	-1.3587	-1.1389		108.519	0.126
C	5.2067	-2.3320	-1.6756		112.391	0.001
C	4.8052	-3.6753	-1.6784		117.096	0.039
C	3.5676	-4.0324	-1.1702		123.677	0.122
C	2.6884	-3.0540	-0.6373		129.766	0.019
N	3.1695	-1.7357	-0.6030		134.377	0.256
H	5.4616	-4.4364	-2.0951		140.18	0.071
H	6.1514	-1.9995	-2.0875		151.183	0.117
H	3.2076	-5.0563	-1.1744		152.219	0.203
O	2.3565	-0.8539	-0.0066		168.22	1.431
O	1.5208	-3.2743	-0.1919		169.081	0.353
C	4.8443	0.0857	-1.2170		171.683	0.614
O	5.9555	0.3209	-1.7179		175.687	0.742

N	4.0163	1.0592	-0.7745		179.642	0.655
H	3.1671	0.7459	-0.2988		189.524	0.237
C	4.4303	2.4574	-0.8390		194.95	0.089
H	5.1951	2.6549	-0.0786		206.681	0.014
H	4.9091	2.5999	-1.8127		210.529	0.085
C	2.1051	1.1785	3.1290		216.914	0.013
C	2.5655	0.9739	4.4240		219.118	0.099
C	2.0559	-0.0972	5.1743		222.958	0.151
C	1.1724	-0.9909	4.5927		225.721	0.059
C	0.7527	-0.8337	3.2441		237.753	0.067
N	1.1565	0.3518	2.6016		242.353	0.257
H	2.3882	-0.2503	6.1987		247.294	0.302
H	3.3503	1.6191	4.8020		273.871	0.221
H	0.8021	-1.8663	5.1167		290.029	0.356
O	0.6105	0.5984	1.4046		297.649	0.226
O	0.0559	-1.6550	2.5815		309.827	0.218
C	2.8270	2.1749	2.2442		310.452	0.118
O	4.0553	2.0634	2.1711		315.252	0.238
N	2.1381	3.1515	1.5774		317.623	0.054
C	2.9512	4.0220	0.7123		329.895	0.21
H	2.4065	4.9570	0.5829		334.128	0.056
H	3.8896	4.2594	1.2271		337.786	0.069
C	-4.6657	-1.8050	0.3498		338.74	0.136
C	-5.5626	-2.7761	-0.0803		357.897	0.162
C	-5.0849	-3.9988	-0.5729		388.028	0.158
C	-3.7215	-4.2267	-0.6589		393.272	0.117
C	-2.7875	-3.2436	-0.2397		396.019	0.054
N	-3.3226	-2.0720	0.3202		407.425	0.042
H	-5.7859	-4.7606	-0.9073		421.037	0.092
H	-6.6168	-2.5324	-0.0351		425.495	0.208
H	-3.3080	-5.1459	-1.0616		432.634	0.019
O	-2.4276	-1.2181	0.8245		445.312	0.043
O	-1.5251	-3.3396	-0.3231		455.725	0.259
C	-5.2346	-0.4552	0.7516		458.828	0.592
O	-6.4591	-0.3447	0.9134		468.991	0.309
N	-4.3704	0.5859	0.8409		478.155	0.174
H	-3.3780	0.3564	0.7485		484.637	1.571
C	-4.8376	1.9346	1.1276		494.075	0.136
H	-4.1514	2.3915	1.8518		497.625	0.114
H	-5.8068	1.8275	1.6197		506.619	0.019
C	3.2684	3.4622	-0.6946		508.36	0.013
H	2.3590	3.0464	-1.1429		510.604	0.047

H	3.5338	4.3370	-1.3026		514.778	0.085
C	0.8204	3.5681	2.1169		520.332	0.021
H	0.2100	2.6659	2.1889		526.28	0.004
H	0.9650	3.9573	3.1351		528.228	0.007
C	0.0298	4.6344	1.3439		533.065	0.005
H	0.6087	5.5608	1.2533		535.049	0.033
H	-0.8082	4.8885	2.0084		575.874	0.135
C	-0.5606	4.2549	-0.0255		580.156	0.172
H	0.2298	4.1008	-0.7679		584.897	0.246
H	-1.1494	5.1111	-0.3785		593.562	0.321
C	-3.8107	3.7400	-0.4903		623.788	0.64
H	-4.1236	4.3980	-1.3067		627.579	0.385
H	-3.5391	4.3744	0.3613		631.577	0.328
C	-5.0067	2.8481	-0.1111		644.169	0.29
H	-5.2949	2.2406	-0.9727		646.394	0.255
H	-5.8442	3.5323	0.0831		650.456	0.158
Am	-0.0579	-1.4161	0.1294		651.881	0.193
					655.813	0.636
					680.714	0.575
					686.829	0.967
					689.938	2.353
					699.658	0.347
					725.544	0.276
					729.184	0.096
					730.495	0.239
					730.913	0.195
					743.582	0.435
					746.168	1.18
					756.555	0.554
					760.585	0.869
					760.965	0.533
					776.113	0.062
					785.516	0.32
					792.44	0.602
					793.979	0.503
					799.011	0.029
					805.573	0.571
					807.911	0.529
					808.851	0.18
					834.136	0.616
					837.903	0.35
					839.292	0.328

					843.105	0.349
					846.607	0.105
					852.053	0.033
					860.88	0.202
					876.365	0.007
					876.796	0.055
					878.816	0.004
					885.706	0.103
					900.475	0.354
					922.553	0.372
					930.335	0.251
					946.487	0.607
					947.376	0.108
					954.711	0.033
					958.884	0.006
					961.2	0.141
					964.093	0.013
					965.39	0.012
					999.031	0.276
					1006.788	0.177
					1008.924	0.024
					1014.466	0.314
					1052.363	0.048
					1068.64	0.039
					1078.248	0.025
					1081.509	0.151
					1083.524	0.254
					1086.515	0.283
					1086.974	0.093
					1088.47	0.081
					1099.267	0.193
					1103.205	0.231
					1110.792	0.21
					1116.684	0.104
					1125.386	0.18
					1161.924	1.333
					1163.153	0.806
					1163.735	1.588
					1164.778	0.516
					1178.512	2.923
					1182.769	4.377
					1183.359	3.809

					1198.652	6.531
					1206.032	0.843
					1206.693	0.372
					1210.644	2.159
					1220.199	1.614
					1224.043	1.68
					1225.931	0.47
					1249.321	0.465
					1253.638	0.24
					1254.574	0.018
					1257.679	0.048
					1261.624	0.024
					1264.329	0.317
					1268.899	0.323
					1273.589	0.453
					1295.06	1.864
					1305.433	3.213
					1316.498	0.929
					1319.231	1.609
					1321.482	2.554
					1343.753	0.811
					1346.766	0.874
					1349.473	0.718
					1362.677	0.683
					1378.686	1.701
					1389.27	0.095
					1391.58	1.733
					1399.92	0.197
					1402.81	0.196
					1408.971	0.492
					1412.68	1.111
					1415.201	2.32
					1415.764	0.132
					1417.934	0.16
					1418.309	0.586
					1420.594	0.491
					1438.339	0.924
					1441.02	0.119
					1441.363	0.232
					1447.051	0.457
					1451.01	2.023
					1455.886	0.414

					1470.961	2.373
					1483.318	0.015
					1487.037	0.167
					1488.872	0.387
					1492.961	0.242
					1495.331	1.385
					1507.275	0.046
					1509.928	0.149
					1514.018	0.657
					1518.404	0.366
					1535.941	0.161
					1546.768	6.219
					1559.39	5.378
					1570.908	3.692
					1574.239	6.341
					1577.657	2.974
					1585.267	6.209
					1590.544	0.606
					1592.129	1.341
					1592.367	1.904
					1592.859	0.215
					1654.234	19.429
					1659.447	4.639
					1664.27	21.809
					1674.633	6.225
					1684.867	7.496
					1700.169	8.333
					1708.134	3.268
					1711.947	4.741
					3005.035	0.667
					3029.123	1.14
					3033.936	0.976
					3035.1	0.459
					3041.554	0.393
					3043.911	0.852
					3051.916	1.475
					3054.417	0.749
					3057.485	0.318
					3069.963	1.011
					3072.877	0.841
					3095.89	1.51
					3098.723	0.833

					3102.095	0.418
					3108.688	0.367
					3126.867	0.167
					3129.277	0.45
					3131.455	0.303
					3150.441	0.61
					3181.693	0.745
					3183.8	0.612
					3185.227	0.364
					3185.369	0.804
					3186.279	0.22
					3220.721	0.297
					3221.187	0.213
					3221.482	0.104
					3223.629	0.127
					3231.335	0.107
					3234.997	0.047
					3247.488	0
					3247.796	0.083
					3430.261	5.454
					3434.183	5.903

Supplementary Table 10

Lifetime measurements for the [$^{249}Bk^{IV}$**1**] in H_2O/D_2O mixtures.

Solvent	Lifetime 1 (μs)	Lifetime 2 (μs)
100% H_2O	187.5	6.7
67% H_2O + 33% D_2O	231.8	7.7
33% H_2O + 67% D_2O	277.8	11.5
100% D_2O[a]	324.0	13.5

[a] extrapolated from linear regressions of the lifetimes in H_2O/D_2O mixtures (τ_1 = 1.3682*%D_2O + 187.2. r^2 = 0.9999. τ_2 = 0.0732*%D_2O + 6.19. r^2 = 0.9003.

Supplementary Table 11
Crystallography data collection and refinement statistics

Crystallization:	
Ligand	$[^{249}Cf^{III}\mathbf{1}]^-$
Crystallization method	hanging drop
Crystallization conditions	1.2-1.4 M $(NH_4)_2SO_4$ 200 mM Li_2SO_4 100 mM NaAcetate 50 mM NaCl pH = 4.1-4.3
Space group	$P4_12_12$
Cell constants (Å)	a = b = 119.6 c = 108.8
Data Collection:	
Cryopreservative	+ 20% v/v glycerol
Beamline (Advanced Light Source, Berkeley, CA)	5.0.1
Wavelength (Å)	1.0000
Resolution Range (Å)	50.0-2.60 (2.64-2.60)
Unique Reflections	24695 (1220)
Average Redundancy	8.1 (8.1)
R_{merge} (%)	11.1 (48.0)
I/σ(I)	28.2 (3.8)
Structure Refinement:	
Resolution (Å)	50.0-2.70
Number of reflections	
all / test	20852 / 1076
Phasing method	molecular replacement
Search model	1L6M.pdb
R_{cryst} / R_{free}	20.3 / 24.1
No. of non-hydrogen atoms (average B-factor (Å^2))	
Protein	4161 (56)
Ligands	165 (106)
solvent	57 (61)
Rmsd	
Bonds (Å) / Angles (°)	0.01 / 1.66
Estimated coordinate error (Å)	
Maximum likelihood e.s.u.	0.227
Ramachandran values (MolProbity)	
Favored region (%)	97.9
Allowed region (%)	100.0
Outlier region (%)	0
MolProbity Score	1.00
PDB accession code	5KIC.pdb

Note: Numbers in parentheses are for reflections in the highest resolution shell.

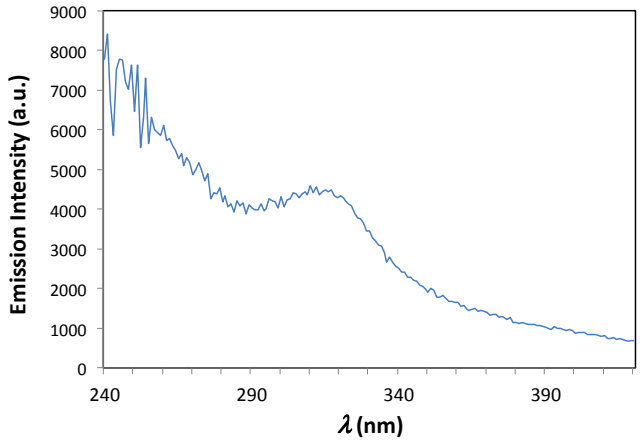

Supplementary Figure 1
Excitation spectrum (λ_{em} = 612 nm) of [Bk^{IV}**1**], in 0.1 M CHES buffer, pH 8.4, 25°C.

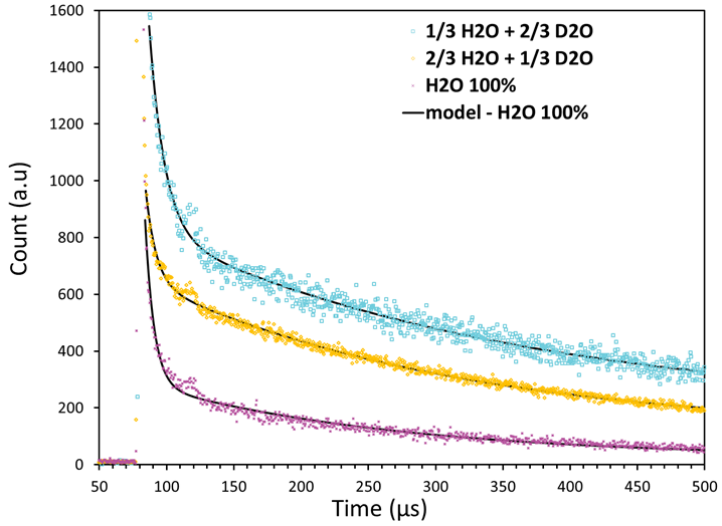

Supplementary Figure 2
Decay lifetime measurements for the [$^{249}Bk^{IV}$**1**] complex in H_2O (magenta crosses), 67% H_2O-33% D_2O (yellow lozenges) and 33% H_2O-67% D_2O (blue squares). Emission at 611 nm after excitation of the ligand at 320 nm. The black solid lines are bi-exponential models with τ_1 and τ_2 given in Supplementary Table 10.

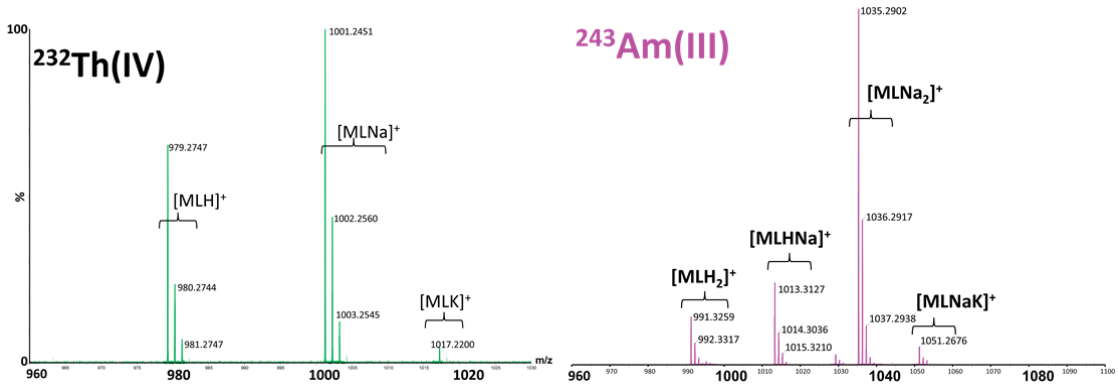

Supplementary Figure 3

High resolution mass spectra of solutions of **1** containing an equivalent of ^{232}Th or ^{243}Am; detection in positive mode.

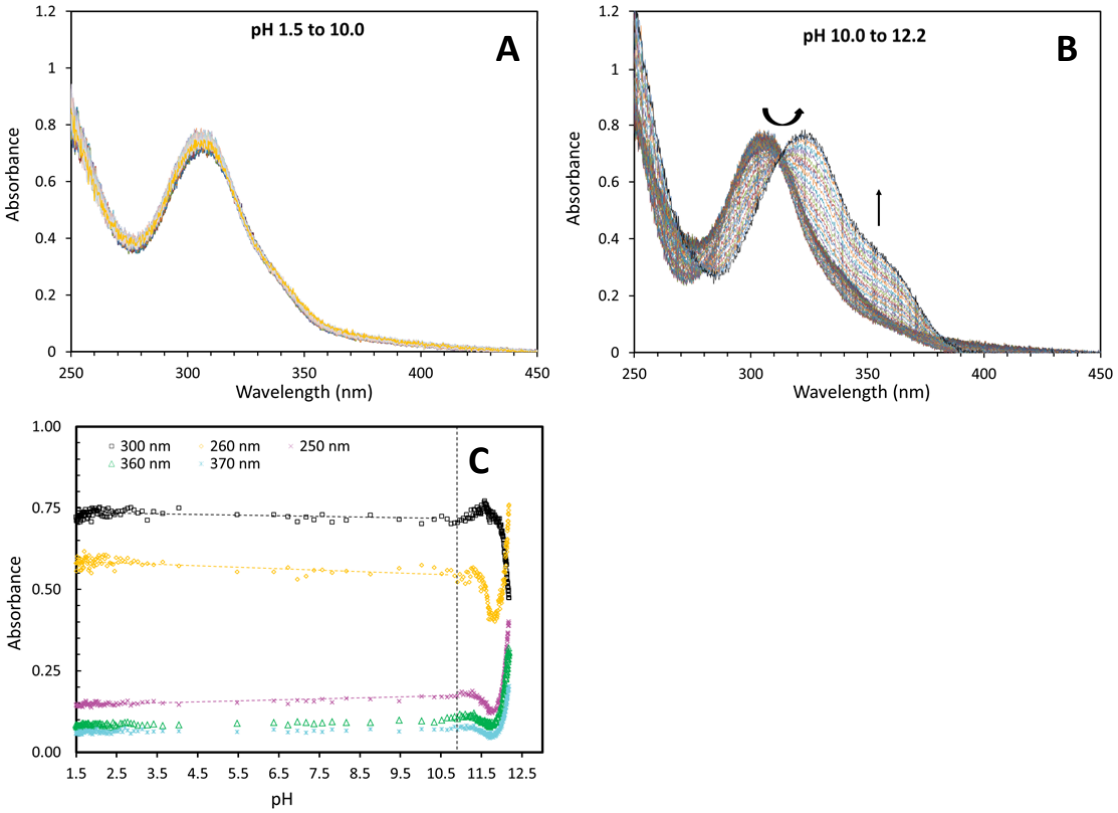

Supplementary Figure 4

(**A**) Absorbance spectra of the complex [Zr^{IV}**1**] as a function of pH. Overlay of 85 spectra measured between pH 1.5 and 10.0 showing the complex stability. (**B**) Overlay of 135 spectra measured between pH 10.0 and 12.2. (**C**) Evolution of the absorbance at 300 nm (squares), 260 nm (diamonds), 250 nm (crosses), 360 nm (triangles) and 370 nm (stars) between pH 1.5 and 12.2. $[Zr]_{total}=[\mathbf{1}]_{total}$ = 55 µM. I = 0.1 M (KCl), T = 25 °C. Path length = 10 mm.

C. Supplementary References

1. P. Y. Chang *et al.*, *J. Chromatogr. Sep. Tech.* **4** (2011), doi:10.4172/2157-7064.1000196.

2. D. H. Goetz *et al.*, *Mol. Cell*. **10**, 1033–1043 (2002).

3. M. Sturzbecher-Hoehne, T. A. Choi, R. J. Abergel, *Inorg. Chem.* **54**, 3462–3468 (2015).

4. B. E. Allred *et al.*, *Proc. Natl. Acad. Sci.* **112**, 10342–10347 (2015).

5. R. J. Abergel, E. G. Moore, R. K. Strong, K. N. Raymond, *J. Am. Chem. Soc.* **128**, 10998–10999 (2006).

6. P. Gans, A. Sabatini, A. Vacca, *Talanta*, 1739–1753 (1996).

7. M. Sturzbecher-Hoehne, B. Kullgren, E. E. Jarvis, D. D. An, R. J. Abergel, *Chem. - Eur. J.* **20**, 9962–9968 (2014).

8. Z. Otwinowski, W. Minor.

9. G. N. Murshudov, A. A. Vagin, E. J. Dodson, *Acta Crystallogr. D Biol. Crystallogr.* **53**, 240–255 (1997).

10. A. Vagin, A. Teplyakov, *J. Appl. Crystallogr.* **30**, 1022–1025 (1997).

11. P. Emsley, K. Cowtan, *Acta Crystallogr. D Biol. Crystallogr.* **60**, 2126–2132 (2004).

12. M. Winn, M. Isupov, G. N. Murshudov, *Acta Crystallogr. D Biol. Crystallogr.* **57**, 122–133 (2001).

13. R. A. Laskowski, M. W. MacArthur, D. S. Moss, J. M. Thornton, *J. Appl. Crystallogr.* **26**, 283–291 (1993).

14. I. W. Davis *et al.*, *Nucleic Acids Res.* **35**, W375–W383 (2007).

15. H. M. Berman *et al.*, *Nucleic Acids Res.* **28**, 235–242 (2000).

16. M. Valiev *et al.*, *Comput. Phys. Commun.* **181**, 1477–1489 (2010).

17. A. D. Becke, *Phys. Rev. A*. **38**, 3098 (1988).

18. C. Lee, W. Yang, R. G. Parr, *Phys. Rev. B*. **37**, 785 (1988).

19. W. Küchle, M. Dolg, H. Stoll, H. Preuss, *J. Chem. Phys.* **100**, 7535–7542 (1994).

20. N. Godbout, D. R. Salahub, J. Andzelm, E. Wimmer, *Can. J. Chem.* **70**, 560–571 (1992).

21. E. Runge, E. K. Gross, *Phys. Rev. Lett.* **52**, 997 (1984).

22. J. Brabec *et al.*, *J. Chem. Theory Comput.* **11**, 5197–5208 (2015).

23. P. J. Hay, R. L. Martin, G. Schreckenbach, *J. Phys. Chem. A*. **104**, 6259–6270 (2000).

24. A. Klamt, G. Schüürmann, *J. Chem. Soc. Perkin Trans. 2*, 799–805 (1993).

25. T. Saue *et al.*, *Release DIRAC12* (2012).

26. K. G. Dyall, *Theor. Chem. Acc.* **117**, 491–500 (2007).

27. X. Cao, M. Dolg, *J. Mol. Struct. THEOCHEM*. **673**, 203–209 (2004).

28. M. Sturzbecher-Hoehne, G. J.-P. Deblonde, R. J. Abergel, *Radiochim. Acta*. **101**, 359–366 (2013).

29. G. J.-P. Deblonde, M. Sturzbecher-Hoehne, R. J. Abergel, *Inorg. Chem.* **52**, 8805–8811 (2013).

30. M. Sturzbecher-Hoehne, P. Yang, A. D'Aléo, R. J. Abergel, *Dalton Trans* (2016), doi:10.1039/C6DT00328A.